Solid Earth, 16, 275–296, 2025
https://doi.org/10.5194/se-16-275-2025
© Author(s) 2025. This work is distributed under
the Creative Commons Attribution 4.0 License.

Solid Earth
Open Access

Paleoseismological evidence of multiple, large-magnitude earthquake surface ruptures on the active Mt. Morrone normal fault, central Apennines, Italy

Irene Puliti[1], Alberto Pizzi[1], Stefano Gori[2], Emanuela Falcucci[2], Fabrizio Galadini[2], Marco Moro[2], and Michele Saroli[2,3]

[1]Dipartimento InGeo, Università G. d'Annunzio di Chieti-Pescara, Chieti, Italy
[2]Istituto Nazionale di Geofisica e Vulcanologia, INGV, Rome, Italy
[3]DICeM, Università degli Studi di Cassino e del Lazio meridionale, Cassino, Italy

Correspondence: Irene Puliti (irene.puliti@unich.it)

Received: 29 July 2024 – Discussion started: 29 August 2024
Revised: 14 January 2025 – Accepted: 26 January 2025 – Published: 13 May 2025

Abstract. The active Mt. Morrone Fault (MMF) and the related Sulmona intermountain basin constitute one of the most characteristic examples of the extensional tectonic landscape carving the central Apennines (Italy). Above the ∼22 km MMF, thousands of inhabitants concentrate on a thriving reality and a historical and cultural heritage of great significance. According to current knowledge, the last activation event of the whole MMF occurred ∼2000 years ago, and the maximum expected magnitude is M 6.6–7.0. Thus, the MMF today constitutes one of the most problematic structures in the central Apennines seismotectonic setting in terms of large-magnitude earthquake probability. Despite this, information on the activity of the MMF is presently relatively sparse, both for associated historical seismicity and paleoseismological data. To strengthen these knowledge weaknesses, we performed new extensive paleoseismological analyses (employing four trenches) in the central sector of the fault. Our goal was to supplement the limited existing dataset, constituted by a single paleoseismological study close to the northwestern tip of the fault. Additionally, we aimed to incorporate findings from a pair of studies focused on archaeoseismological and speleoseismological secondary evidence. Through these analyses, we unveiled four significant surface rupture events of the MMF, three of which occurred over the past 6000 years BP. Specifically, the youngest identified event occurred after 3.6–3.5 kyr BP, thus being chronologically consistent with the event in the second century CE, a penultimate event after 4.4 kyr BP, a previous event that occurred after 5.4–5.3 kyr BP, and the oldest event that took place after 9–8.9 kyr and (presumably) before 5.8–5.7 kyr BP. Considering that the estimated cumulative minimum vertical displacement encompassing the last three events is ∼140 cm, and based on the length of the fault at the surface, we can confirm that earthquakes with M 6.6–7.0 may be expected from the activation of the MMF with an inferred average recurrence interval not longer than 1800 years over the last ∼5.4 kyr.

1 Introduction

The main parameters useful for fault-based seismotectonic analyses of seismically active regions are the magnitude, the recurrence interval of past earthquakes on a fault, the last event of fault activation, and the fault geometry (McCalpin, 2009). Studying the Holocene seismic history of a fault constitutes a necessary task to improve our knowledge of how the fault has ruptured in the past and how it might behave in the future. Therefore, answering the question of the Holocene rupture history (from which the repeat of maximum credible earthquakes is to be derived) for each fault of a given system is a relevant goal to achieve.

However, linking the magnitudes of historical earthquakes to a particular active fault is often challenging and depends on the quality of historical catalogues and the conservation of the geological traces of fault ruptures in the landscape.

In this regard, the Sulmona basin is bounded by one of the major active normal faults of the central Apennines, the so-called Mt. Morrone Fault (hereafter MMF). The basin was hit by several historical earthquakes of $M_w > 5.7$ and up to about M_w 7, generated by adjacent seismogenic sources (Rovida et al., 2022; Fig. 1). Nonetheless, no large magnitude (of up to 6.5–7) is presently associated with the MMF activity, though the origin of some of them is still debated. Such uncertainty stimulated researchers to investigate the seismic history of the MMF and its seismogenic behavior, at either long- or short-term scales.

In the absence of recent occurrences of seismic events, evidence of paleoearthquakes on active faults can be derived from paleoseismological investigations (e.g., Manighetti et al., 2007; DuRoss et al., 2016). On the other hand, trenching provides punctual information that might not be representative of the entire fault system deformation because both coseismic and long-term slip distribution can vary significantly along the length of a fault, especially across complexities (e.g., Iezzi et al., 2018, 2023; Puliti et al., 2020). Indeed, different potential scenarios of the distribution of surface ruptures can occur during earthquakes along the causative fault, due to several possibly interacting factors not easily discernable a priori. For instance, the seismic histories derived by trenches may also suffer from non-preservation of coseismic surface ruptures due to erosional processes or sedimentary hiatuses.

At present, a sole paleoseismological investigation has been conducted on the MMF by Galli et al. (2015), from which four paleoearthquakes over the last ~ 9 kyr have been retrieved. However, this represents an isolated spot located in the northern portion of the fault, and therefore it might not provide a compelling picture of how the fault ruptured and what the maximum expected event is (in terms of fault surface offset and of the related expected magnitude).

In this regard, the present study focuses on enlarging the paleoseismic records of the MMF and extending back the seismic history retrieved. Here we show the results of paleoseismological investigations performed on a different portion of the same fault, that is, at the central portion of the MMF, close to the Roccacasale village (Fig. 2), which, according to the classical fault evolution model, is expected to record the highest vertical displacement (e.g., Walsh and Watterson, 1987; Peacock and Sanderson, 1991), thus providing more significant pieces of evidence regarding the actual surface displacement potential (that can be related to the maximum earthquake size generated by the fault; see, e.g., Wells and Coppersmith, 1994). Here we describe the results of the new paleoseismological analysis performed along the MMF through four trenches dug in a sector of the fault trace well expressed in the local morphology. As shown in the discussion, the analysis of the obtained results allows us to attempt to define the fault rupture's dimensions and geometry and the timing of seismic events, which should be more representative of the maximum behavior of the fault. Finally, we discuss these results and observations in comparison with the existing paleoseismological study (i.e., Galli et al., 2015) to unravel the short-term fault deformation at a system scale.

2 Regional tectonic setting

The Apennine chain results from the complex interaction between the African and European plates and the Adria microplate since the late Oligocene–Miocene. The westward subduction of the Adriatic lithosphere beneath Europe and its progressive eastward flexural retreat produced an NE-verging foreland thrust-and-fold system involving Mesozoic–Cenozoic carbonate rocks in the central Apennines with a contemporaneous back-arc opening of the Tyrrhenian Sea (Boccaletti et al., 1990; Cipollari et al., 1999; Cipollari and Cosentino, 1995; Doglioni, 1991; Patacca et al., 1990). The contractional structure is characterized by NW–SE-striking anticlines bordered at their forelimbs by gently southwest-dipping thrust fronts (Ghisetti and Vezzani, 1997). Since the Late Pliocene–Early Pleistocene, SW–NE extensional tectonics overprinted the contractional deformation, with active normal faults generally trending parallel to the chain axis and dipping to the SW, affecting the axial zone of the chain, and becoming progressively more recent toward the Adriatic foreland (i.e., to the east) (e.g., Lavecchia et al., 1994; Piccardi et al., 1999; Galadini and Messina, 2004). Alongside newly formed normal faults, the extensional deformation also re-used fault planes inherited from the compressive phase (Calamita and Pizzi, 1992; Cavinato et al., 1994; Falcucci et al., 2018; Pucci et al., 2019).

In the central Apennines, the activity of normal fault systems has led to the formation of several graben or half-graben structures corresponding to intermountain basins (e.g., Fucino, Sulmona, L'Aquila, and Norcia basins) located in the hanging walls of the main normal faults. These basins hosted continental depositions filled with Plio-Quaternary successions (e.g., Bosi and Bertini, 1970; Bosi et al., 2003; Pucci et al., 2015; Puliti et al., 2022) (Fig. 1). The normal fault activity over the Quaternary is testified by evidence of displaced continental deposits and landforms. The present extensional activity is also testified by the historical seismicity (earthquakes with magnitudes of up to 7.0 in the past millennium, e.g., Rovida et al., 2022) and instrumental seismological data (e.g., Chiaraluce et al., 2017; Pondrelli et al., 2010; Ekström et al., 1998), which indicate earthquake ruptures compatible with extensional faulting, and by several studies dealing with active tectonics and paleoseismology (e.g., Galadini and Galli, 2000; Galli et al., 2008).

2.1 Geological setting of the Mt. Morrone Fault (MMF)

The Mt. Morrone ridge is in the outer portion of the central Apennine range. It represents an anticline structure related to northeast-verging thrust that was active during the late

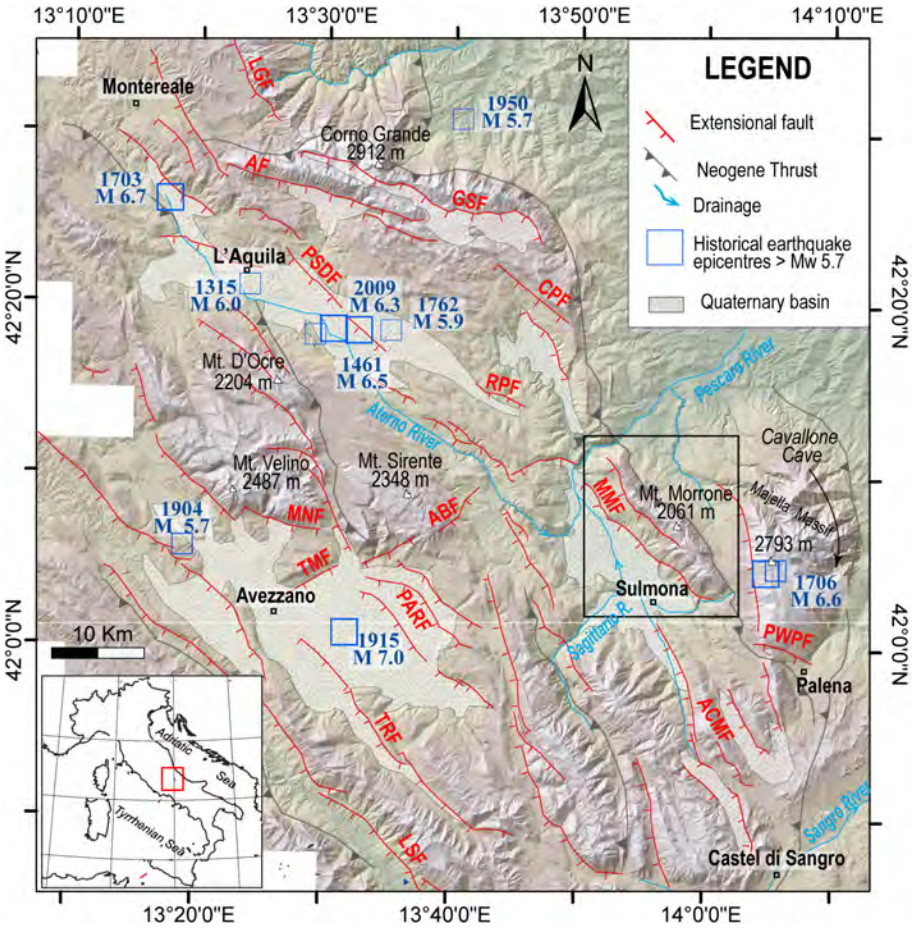

Figure 1. Structural framework of the Abruzzi region and historical seismicity of the Abruzzo region fault systems modified after Puliti et al. (2024); acronyms define faults considered as active: Laga–Gorzano Fault system (LGF), Gran Sasso Fault system (GSF), Assergi Fault (AF), Mt. Cappucciata Fault (CPF), Paganica San Demetrio Fault system (PSDF), Roccapreturo Fault (RPF), Magnola–Velino Fault (MNF), Tre Monti Fault (TMF), Parasano Fault (PARF), Trasacco Fault (TRF), Liri Southern Fault (LSF), Mt. Morrone Fault (MMF), Aremogna–Cinque Miglia Fault system (ACMF). The Palena–western Porrara fault (PWPF) is from Pizzi et al. (2010). The Avezzano–Bussi Fault (ABF) is from Gori et al. (2017). The shaded relief derives from a 20 m DEM. Historical earthquake epicenters ($>M_w5.7$) are from catalogue CPTI15 (Rovida et al., 2022). Major Neogene thrusts are indicated in grey (Ghisetti and Vezzani, 1997). The investigated area is outlined by the black rectangle.

Messinian to the Early Pliocene (e.g., Cipollari and Pipponzi, 2003). The thrust fault, outcropping along the eastern limb of Mt. Morrone, superimposed Mesozoic–Cenozoic limestones over Cenozoic (Neogene) terrigenous deposits (Fig. 2).

The back limb of the Mt. Morrone anticline was then affected by a ∼ 22 km long, NW–SE-striking normal fault giving rise to the Sulmona basin, a ∼ 7 km wide half-graben intermontane depression that bounds the Mt. Morrone ridge all along its length (e.g., Gori et al., 2011; Puliti et al., 2024). The Sulmona basin is filled with Quaternary sedimentary succession, which has been described in several studies (e.g., Demangeot, 1965; Vittori and Cavinato, 1995). According to them, the depression has hosted a fine-grained lacustrine deposition >400–500 m thick since the Early Pleistocene (Cavinato and Miccadei, 2000; Giaccio et al., 2009; Miccadei et al., 1998). Afterwards, the continental sedimentation was dominated by an Upper Pleistocene coarse-grained alluvial sedimentation mainly driven by the Vella, Gizio, Sagittario, and Aterno rivers and by the drainages from the Mt. Morrone western flank. The southern area of the Sulmona basin has also been affected by landslide deposits derived from large-scale gravitational movements that occurred from the Early to Late Pleistocene, according to the available literature (e.g., Miccadei et al., 1998; Gori et al., 2014).

The extensional active MMF comprises two main parallel fault branches from Popoli to Pacentro, the western and eastern fault branches (e.g., Gori et al., 2011 and references therein), whose related scarp is found at different elevations along the slope (400–800 and 1200–1500 m a.s.l. respectively). The highest and easternmost branch, defined as the "Schiena d'Asino Fault" (Ciccacci et al., 1999; denoted SAF hereafter), is located at the foot of the Mt. Morrone peak, and

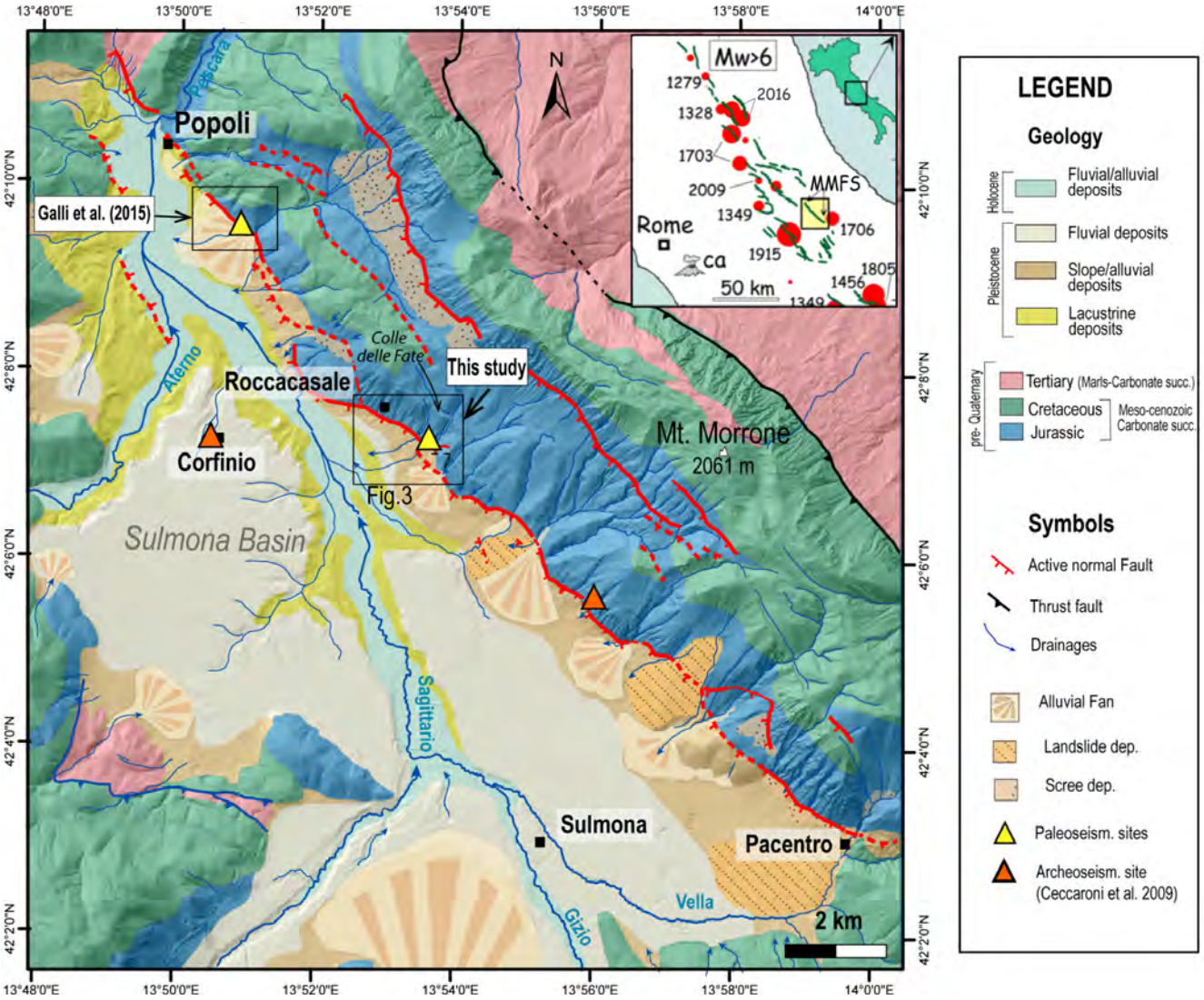

Figure 2. Simplified geological map of the Mt. Morrone Fault (MMF), modified from CARG geological sheet "369 Sulmona" (Servizio Geologico d'Italia, 2006). Locations of the paleoseismological study of Galli et al. (2015) and this study are reported (Fig. 3), and yellow triangles indicate the excavation sites. The orange triangles are some of the archaeological sites reported in the archaeoseismological study by Ceccaroni et al. (2009). In the inset: the locations of primary active faults in central Italy and $6 < M_W < 7$ earthquakes are shown, modified from Galli et al. (2015). The yellow rectangle marks the area in which the MMF is located.

it is made of an at least 14 km long main bedrock fault scarp on the central–northern portion of the mountain range at the base of which the fault plane is nearly continuously exposed.

The western fault branch is located at lower elevation, and it bounds the Sulmona basin all along its extent. It strikes N140° from the northern tip up to the central portion (north of the Roccacasale village) and N155° southward. Locally, some splays of 0.5–1 km of length, like the fault portions at Roccacasale, strike from N155° to E–W-oriented. The fault plane is visible at the base of the fault scarp along several sections from Popoli to the north and to Pacentro to the south, of about 3–5 km long each. The kinematic indicators measured along the fault planes show a prevalent normal dip-slip movement; however on the NNW–SSE and near E–W-striking planes a slight left and right oblique component is observed, respectively, in agreement with a main NE extension direction (e.g., Pizzi and Pugliese, 2004). For the basin-bounding fault, a minimum age of 268 kyr BP has been estimated from U–Th dating of carbonate mineralization linked to the coseismic rejuvenation, with a 10–15 kyr cyclicity, of the structural permeability in the fault zone (Vignaroli et al., 2022). By measuring the displacement of the remnants of Early Pleistocene breccias outcropping in a few sites of the basin, a minimum offset of 350 m is estimated to be accommodated by the western fault branch (Gori et al., 2007, 2014; Miccadei et al., 2004). As for the late Quaternary kinematic

history, Late Pleistocene–Holocene deposits are displaced along the western fault splay of up to about 20 m, attesting to a slip rate of the branch on the order of 0.4 mm yr^{-1} (Gori et al., 2011; Puliti et al., 2024).

2.1.1 Historical seismicity and previous paleoseismological investigations of the MMF

The Sulmona area was hit by several historical earthquakes of $M_w > 5.7$ and of up to M_w 7, namely the 1349, 1456, 1706, 1915, and 1933 events (Rovida et al., 2022). However, none of them were associated with the MMF activity but with adjacent seismogenic sources, though the origin of some of them is still debated. An example is the 1706 Majella earthquake tentatively associated with a thrust or backthrust (i.e., west-verging) fault reactivation by some authors (De Nardis et al., 2008; Galli and Pallone, 2019), even if no conclusive data supporting this hypothesis have been found to date. This open issue stimulated researchers to investigate the seismic history of the MMF.

Archaeoseismological investigations on damaged ancient settlements in the Sulmona basin area cast light on the occurrence of a strong local earthquake around the middle of the second century CE (Galadini and Galli, 2001; Ceccaroni et al., 2009). From the reconstructed shaking scenario, a consistency between the event and the activation of MMF has been found. The written source related to this earthquake is represented by an epigraph mentioning the restoration of a damaged weighing house at an ancient locality about 18 km north of Sulmona. In the available seismic catalogues, it is reported with the conventional date of 101 CE, an epicentral intensity I_0 9–10 of the MCS scale, and an estimated magnitude M_w 6.3. Faulting evidence and radiocarbon dating from paleoseismological trench studies close to Popoli (see location in Fig. 2) performed by Galli et al. (2015) corroborated the occurrence of MMF activation in a period consistent with the second-century AD seismic event, besides three prior faulting events, which occurred in the past $\sim$9 kyr BP, with the most recent constrained, indeed, as the middle of the second century CE.

On a regional scale, the MMF has also been associated with seismic events recorded on speleothems in the Majella Massif (Cavallone Cave, Fig. 1; Di Domenica and Pizzi, 2017). In the cave, large collapses of cave ceilings, fractures, broken speleothems, and radiocarbon dating of new re-growing stalagmites on their top, together with other coeval off-fault geological data collected in surrounding areas outside the cave (i.e., wooden samples in the Palena rock avalanche), provide important constraints for the individuation of a mid-Holocene paleoearthquake that occurred around 4.8–4.6 kyr BP and post 5.4–5.3 kyr BP, respectively (Di Domenica and Pizzi, 2017). The authors also postulated the observed effects on speleothems were caused by an earthquake with a magnitude larger than that supposed by the activation of the sole MMF, hypothesizing the conterminous rupture of other nearby active faults, causing earthquakes of magnitude around 7. In this perspective, assuming that the MMF is a "segment" of a larger seismogenic source comprising also the Palena and western Mt. Porrara active normal faults (PWPF in Fig. 1) of Pizzi et al. (2010) and Gori (2010) located just SE of the MMF and aligned with it, Bordoni et al. (2023) calculated that they are capable of rupturing together with earthquakes of M_w of about 7.

3 Paleoseismology of the Monte Morrone Fault system

3.1 Study area

Based on the geological and geomorphological background and the new observations and data acquired in the field, we investigated the central portion of the MMF, close to the Roccacasale village. Here, the western fault splay of the MMF placed the Mesozoic carbonate limestones, in the footwall, into contact with Quaternary alluvial deposits, in the hanging wall (Fig. 3a). The fault is expressed as a 2 km long bedrock fault scarp at the base of which the fault is exposed, with an N110° strike and dipping 50–55° SSW toward the Sulmona basin. The fault zone in the footwall consists of a main slip surface characterized by decimeter-thick cemented cataclasite (Fig. 3b) and a damage zone of several meters to tens of meters affecting the Lower Jurassic dolomitized carbonate bedrock where multiple secondary parallel fault splays accommodate the brittle deformation (Fig. 3c).

The hanging wall block consists of confluent alluvial fans from the slope of Mt. Morrone, leading to a well-stratified alluvial depositional sequence that dips gently towards the Sulmona basin. Basinward, these alluvial fans pass to a paleoalluvial plain sequence, in the literature indicated as the Upper Sulmona Terrace (UST; Miccadei et al., 1998), which represents the ancient alluvial base level of the Sulmona plain. The age of the alluvial deposits is constrained up to 36–40 kyr according to a tephra layer embedded in both the alluvial fan and alluvial deposits, 5 m below the topographic surface (Gori et al., 2011; Galli et al., 2015), and to the exposure dating of the surface by cosmogenic nuclides concentration (Puliti et al., 2024). Colluvial sediments locally cover the alluvial bodies.

Stream incisions cutting through the alluvial sedimentary bodies show the presence of several synthetic and antithetic fault strands affecting these deposits, close to the main fault zone. They reflected in the morphology of the hanging wall, where field observations and morphostructural study highlighted the presence of further fault scarps of $\sim$10–20 m length, parallel to the main carbonate one. Unfortunately, most of these scarps have been severely altered by widespread agricultural practices over centuries. Indeed, human activity has obscured or re-elaborated a large part of the cumulative fault scarps, leaving only a few sites where rel-

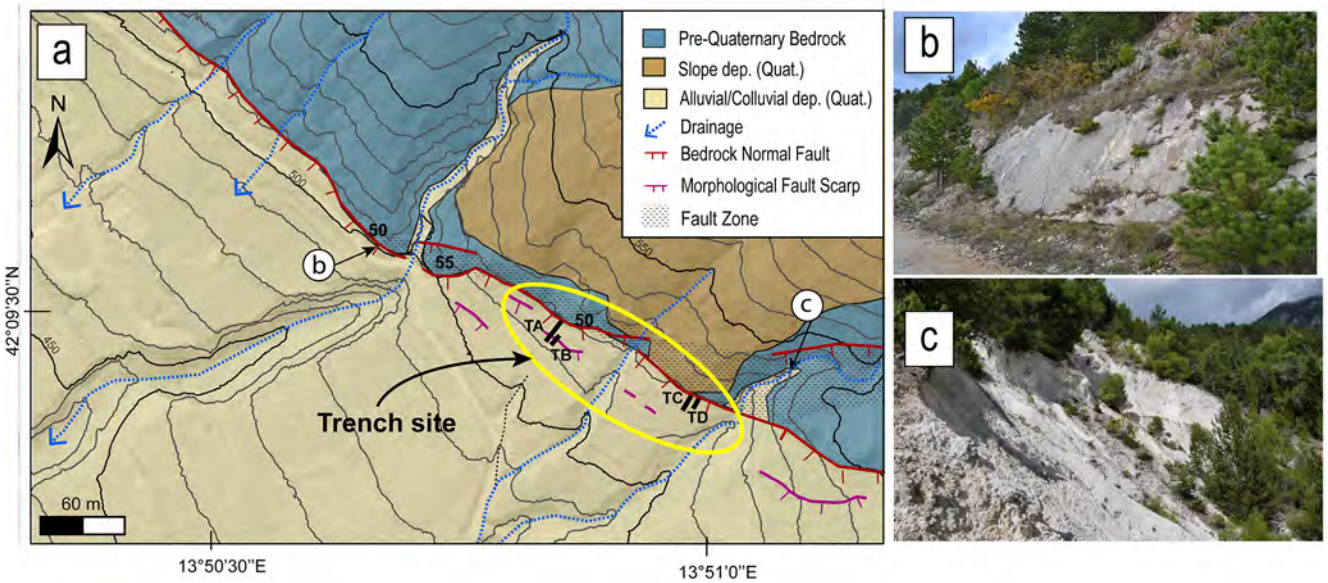

Figure 3. (a) Simplified geological map of the study area. The four trenches are indicated by the black segments within the yellow ellipse. The contour lines are 10 m each, and the locations of the field pictures are indicated. **(b)** Field picture of the cataclasite at the Roccacasale fault main slip plane outcropping along the road. **(c)** Field picture of the Roccacasale cataclastic fault zone.

atively undisturbed Late Pleistocene–Holocene morphotectonic features are preserved.

We selected the paleoseismological study site 1 km south of the Roccacasale village. Four trenches, named TA, TB, TC and TD, have been excavated with an N 35° orientation, that is perpendicular to the fault scarps (Figs. 3 and 4). The 20 m long TA trench was opened from the bedrock fault plane and across a minor fault scarp, located 15 m far from the main one. A shorter 6 m long trench, TB, was dug 4 m southward, far from trench TA. Two further 5 m long trenches, TC and TD, were excavated 100 m SE of TA and TB, 5 m apart from one another; their location was chosen at the base of the fault plane involving slope breccias and alluvial fan deposits at the footwall. The walls of the four excavations were cleaned and gridded at 1 × 1 m spacing (locally 0.5 × 0.5 m) and prepared for stratigraphic logging and geochronological sampling.

We performed radiocarbon dating of organic material and charcoal shards incorporated in the sediments to obtain chronological constraints for the stratigraphic sequences exposed by the trenches. Further, our radiocarbon samples (charcoals and bulk) were sent to two different specialized laboratories (Beta Analytic Laboratory, Florida, USA, and CEDAD – Centro Datazione e Diagnostica of Salento University, Italy). The measurements were performed through accelerator mass spectrometry (AMS) analysis and calibrated through BetaCal3.21 and OxCal3.10 in the two laboratories. The radiocarbon ages used in this work have been corrected according to Ramsey (2009) and Reimer et al. (2013) and then reported as BP.

3.2 The TA and TB trenches

3.2.1 Stratigraphic setting of TA and TB and chronological constraints

In this section we analyze the stratigraphic and tectonic setting of the TA and TB trenches and present the results of radiocarbon ages used to constrain the Holocene paleoseismological history. Some of the units exposed by the two trenches were comparable by sedimentary characteristics, which, also considering the proximity of the two sites, suggests a shared stratigraphy. We distinguished eight stratigraphic units whose order follows their chronostratigraphic position numbered from 1, the oldest in both excavations, up to 8, the youngest (Figs. 5 and 6). We also identified and labeled the sediments filling the paleofissures as "Fi", which, as discussed below, we associated with subsequent fault activation events (e.g., Fi4 associated with paleoearthquake Eq4). We labeled additional infilling sediments that could be older than Fi4 as FiX and FiY, but the lack of the complete geological record prevents any chronological constraint of these infilling units.

The oldest depositional body of the stratigraphic sequence is unit U1, outcropping in trench TB. It is made of interfingered slope and alluvial fan deposits and comprises whitish and carbonate-stratified breccias containing orange, sandy levels that are 20 cm thick and dipping 15°.

Unit U2 is made of light-yellow calcareous sand at the base with a coarsening upward trend, matrix-supported with very small clasts up to 2–3 mm in the upper part. This unit

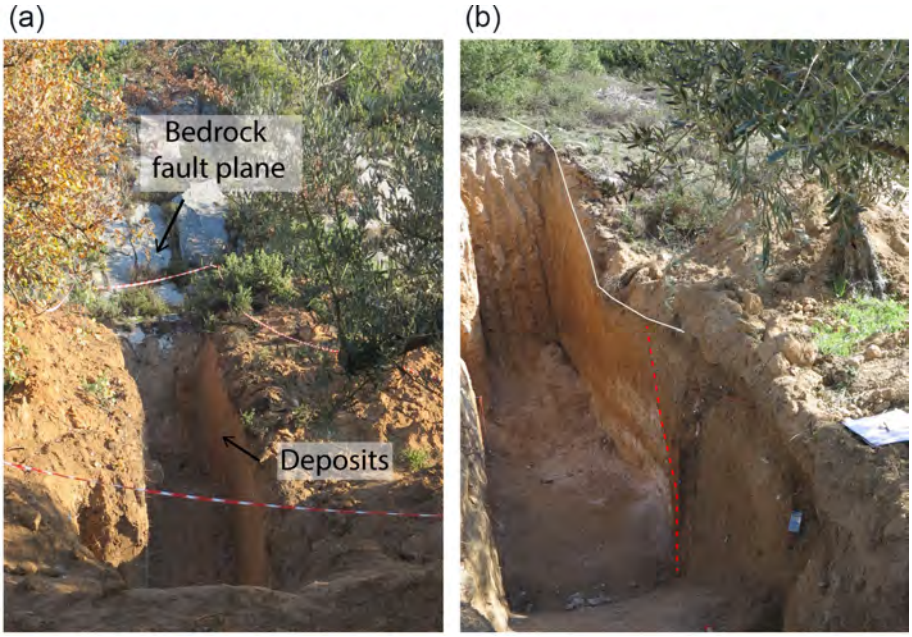

Figure 4. Field pictures of **(a)** trench TA and **(b)** trench TB.

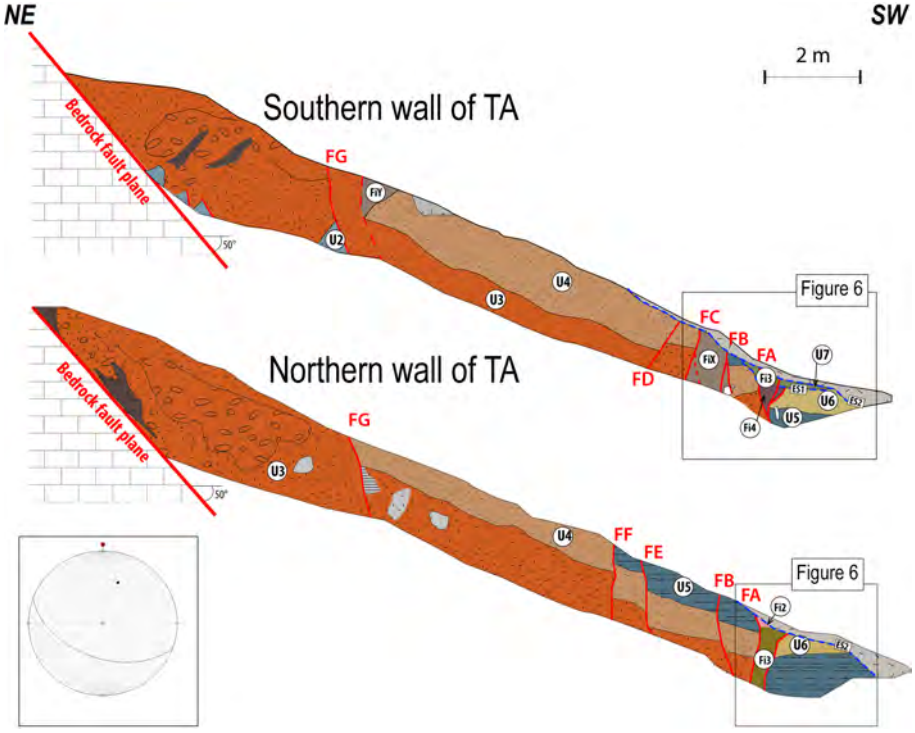

Figure 5. Stratigraphic sketch logs of trench TA's southern and northern walls. The northern wall log is mirrored (to its actual appearance) to highlight the correspondence between the two walls. The stereo plot indicates the bedrock fault plane measured at the top end of the trench (200/50). Units and faults, marked by red lines, are labeled in the figure.

outcrops in small patches at the base of the southern wall of trench TA.

Upward, the stratigraphic sequence continues with unit U3, found extensively along the entire TA trench walls: a medium-to-fine calcareous sandy deposit that is red to orange, with sparse and small clasts (5 mm) and an average thickness of 60–70 cm up to 2 m close to the bedrock fault plane. U3 shows continuity along the TA trench walls, with a coarsening upward texture and an upward increase in consolidation. The massive aspect and thickness of sandy deposits were recognized to be associated with sediment-laden processes, producing hyper-concentrated sandy slope deposits (Benvenuti and Martini, 2009). Commonly, in continental systems, these sands are matured and temporarily stored in coeval continental depositional environments, where they are periodically removed and transferred into the basin by rivers during major floods (Zavala, 2020).

The subsequent unit U4 shows a thickness of 40–75 cm, composed of very coarse calcareous sand that is nuanced from orange to hazelnut. It is a dense deposit with small clasts from 2 to 10 mm organized in small patches and abundant reworked tephra minerals. A 10 cm thick coarse layer, thinning eastward, marks the contact with the unit below.

The southwesternmost portion of the excavation of TA (Fig. 6) and trench TB exposed the youngest preserved deposits, all represented by fine-grained colluvial deposits with an attitude conformable to the slope. Unit U5 is a silty colluvium with yellowish-brown/grey sand, having ~ 100 cm of minimum thickness, with rare carbonate clasts. The base of unit U5 is characterized by a gravel matrix-supported layer with clasts from 1 to 10 mm (locally sub-rounded) and parallel to the main deposition direction.

Unit U6 is a sandy brown-to-yellowish 55–65 cm thick massive colluvium with a few clasts less than 1 cm in diameter. U7 is a deposit composed of an unstratified well-consolidated clast-supported part with 20 cm of thickness, and then, in its westernmost position, it is a more yellowish sandy deposit 20–25 cm thick, less consolidated with small, rounded carbonate clasts of 1–2 cm diameter. Radiocarbon dating of charcoal sampled in U7 provided an age of 5830–5749 years BP (sample RC2). Given the colluvial origin of the sediments, this age defines a lower chronological limit for the deposition. Two erosional surfaces, named ES1 and ES2, mark two unconformities between U6 and U7 deposition, and between U7 and the plowed soil, respectively. The occurrence of the erosional surface ES2, with anthropogenic genesis due to agricultural activities, prevented the preservation of the uppermost unit U8, of which we have evidence of its presence only in the infilling sediment Fi3 described below, which also occurs at the expense of this eroded unit. Specifically, U8 was mainly composed of a dark-brown paleosol, from which we collected charcoal fragments that gave an age of 4985–4963 years BP (sample RC1, Table 1).

As exposed before, the trench walls showed fissures infilled with sediments from the adjacent units. Specifically, based on the material contained, four different infilling deposits were identified. In trench TA (Figs. 5 and 6), the FiY and FiX are both grey-hazelnut silty sands related to U3–U5, and U3–U4–U5 re-elaboration, respectively; the Fi4 is a dark-grey silty sand with scarce carbonate clast of 1 cm in size with a parent material related to units U5–U6. FiY, FiX and Fi4 can be only observed on the southern wall of TA.

The Fi3 unit is a dark-brownish silty sand with local yellowish sandy patches. In the northern wall, Fi3 showed several patches of dark colluvium with carbonate pebbles of 5–10 cm in size. The parent material of Fi3 might be related to units U5–U6–U7 and to the younger unit U8, which, as described above, should have been a dark-brown paleosol removed during the erosional phase marked by the surface ES2 and preserved only as Fi3 infill. Charcoal samples from two fissures in TB, but with the same stratigraphic position and infill material as that of Fi3 in TA, have been radiocarbon dated. In order to avoid any possible bias, the two samples were sent to two different laboratories (i.e., Beta Analytic and CEDAD). The validity of the hypothesis was confirmed by the large overlap of the date ranges obtained: 5424–5320 years BP for the sample RC3 analyzed by CEDAD and 5458–5375 years BP for the sample RC4 analyzed by Beta Analytic (see Table 1), indicating that the infilling deposit of Fi3 occurred after the younger age of the two. The Fi3 deposited above Fi4.

Fi2 has been only observed at the northern wall of TA (Fig. 6). It is filled by a silty colluvial deposit unconformably overlaying Fi3. The radiocarbon age determination of a charcoal shard contained in it gave an age of 4985–4862 BP. From lithological observations the parent material of Fi2 might be related to U7 and U8. The sequence is truncated at the top by the ES2 erosional surface and sealed by thin-plowed soil.

3.2.2 Faulting events of trench TA

Trench TA exposed eight normal fault strands, at the hanging wall of the main bedrock fault plane, arranged both as synthetic (faults FA, FB, FC, FE, FF, and FG in Fig. 5) and antithetic (faults FD in Fig. 5) splays to the main fault. Fault FA was in the westernmost portion of the trench (Fig. 6) and displaced the youngest units of the stratigraphic sequence. Based on the exposed stratigraphy and the structural relations observed on the trench walls, we determined several faulting events from the displacement of different deposits and filled coseismic fissures.

On both trench walls, a well-expressed ~ 60 cm wide subvertical fault zone associated with FA has placed units U3–U4–U5 in contact to the east, with U5–U6–U7 to the west. These units were involved in the fault zone where there was evidence of a back-tilting of the hanging wall units in the northern wall and of the footwall units in the southern wall, along the main 50° SW-dipping bedrock fault plane (Fig. 6). Moreover, at the hanging wall of FA, unit U5 incorporated

Table 1. Radiocarbon dating of samples collected in the investigated trenches. Each age is calibrated and with its related probability. See Figs. 6, 8, and 10 for sample locations.

Sample	Trench	Unit	Calibrated radiocarbon age	Dated material	Lab
RC1	TA	Fi2	4985–4862 cal yr BP (80.3%)	Bulk	Beta Analytic
RC2	TA	U7	5830–5749 cal yr BP (58.2%)	Detrital charcoals	Beta Analytic
RC3	TB	Fi3	5424–5320 cal yr BP (47.7%)	Detrital charcoals	CEDAD
RC4	TB	Fi3	5458–5375 cal yr BP (57.7%)	Detrital charcoals	Beta Analytic
RC5	TC	U3	3610 ± 30 cal yr BP (95.0%)	Detrital charcoals	Beta Analytic
RC6	TC	U2	4460 ± 30 cal yr BP (48.3 %)	Detrital charcoals	Beta Analytic

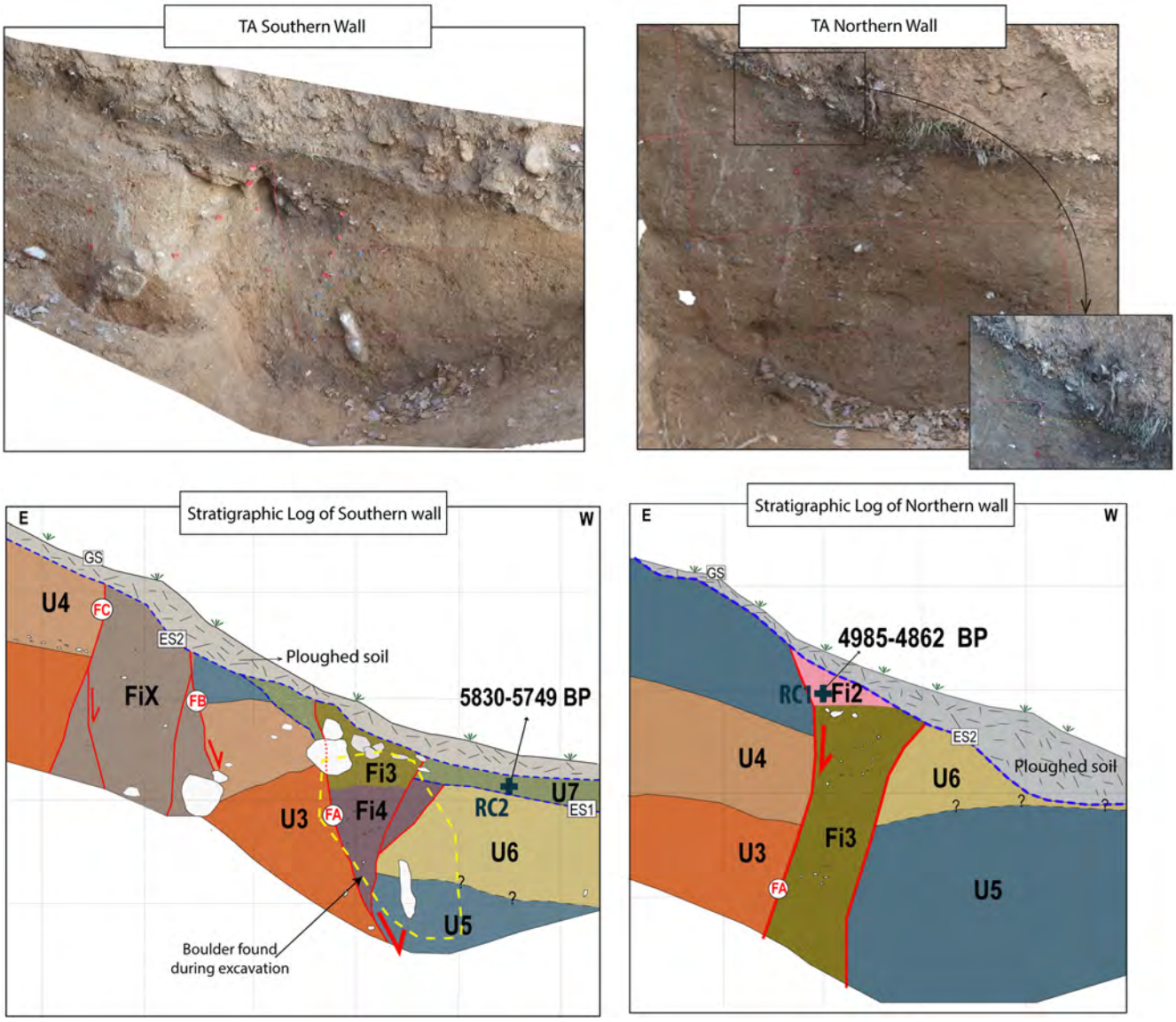

Figure 6. Stratigraphic log of the portion of trench TA and the southern and northern (mirrored) wall. The inset is a zoomed-in picture of the Fi2 colluvial wedge. Unit names and faults are indicated in the figure and referred to in Table 1. ES: erosional surface; GS: ground surface. The sample's position is indicated with a blue cross. The shape of the removed-boulder during excavation is outlined by a dashed yellow line (see text for details). Each grid is 50 cm.

an elongated carbonate block with a long axis of around 50 cm, having an attitude parallel to the fault plane (the white clast drawn in the lower part of the log of the southern wall; Fig. 6). The FA faulting events have determined the formation of fractures that experienced different episodes of opening and subsequent infilling with the collapse of the involved deposits: on the northern wall, the fracture walls defined a funnel shape widening from 25 cm at the base to 50 cm at the top of the exposure; on the southern wall, the fractures had a complex wedge shape tapering downward and merging with fault FA.

A noteworthy aspect of the stratigraphic setting uncovered by trench TA is that a large carbonate boulder was unearthed during the excavation, right along the FA shear zone (in Fig. 6 the shape of the boulder is outlined by a dashed yellow line). The boulder was a little less than a meter long, some tens of centimeters large, and up to 10 cm thick, and the attitude of the long axis defined a roughly vertical position, paralleling the fault zone. The considerable size of the block, the distance from the carbonate bedrock fault scarp (about 15 m apart), the position right in the fault zone of FA, and the attitude (parallel to the fault plane) suggested that it might have been intentionally placed there maybe by anthropic activities aimed at managing this part of the slope (i.e., creating stable terraces for agricultural practices) owing to the presence of a (possibly newly formed) scarp. An alternative but much less probable hypothesis is that the boulder fell from the carbonate scarp, rolled/bounced downslope, and halted almost vertically right on the FA shear zone, with the same attitude as the fault scarp. Unfortunately, the boulder was accidentally removed during the excavation of the trench, so we were not able to accurately define the relationship with the stratigraphic sequence. Nonetheless, we can testify that it was at the contact between the above-described Fi4 and Fi3 units and U3.

As for fault FA, at least four faulting events have been identified since the deposition of unit U6 (as well as an undefined number of faulting events preceding the deposition of unit U6 mostly confined in the older U3, U4, and U5 units), whose succession has been reconstructed in Fig. 7. The layers corresponding to units from U3 to U6 constituted the oldest exposed sediment involved in the FA faulting and recording prior displacement events (Fig. 7a). Units U3–U6 were faulted by event Eq4, fissured, and displaced vertically (Fig. 7b). The opening that occurred was a maximum of 60 cm large, and the filling had a height of 70 cm. The infilling deposit was unit Fi4, composed of a mixed deposit of U5–U6. At the end of this stage (Fig. 7c), the near-vertical free face was removed during the erosional phase that produced ES1, and a debris-facies colluvium (U7) deposition took place subsequently (Fig. 7d). Unit U7 sealed the open fissure, constituting the wash-facies colluvium, and post-dated the first surface rupture observed, Eq4. After unit U7, the deposition of unit U8 occurred, but the following erosional processes prevented its preservation (Fig. 7e).

With earthquake Eq3, U7 and U8 were faulted (Fig. 7f). The fissure that formed as a consequence to Eq3 was infilled by sediment Fi3 from the immediate hanging wall and footwall, hence by a mix of U5–U6–U7–U8 deposits (Fig. 7g). By assuming the same faulting events occurred on the two trench walls, we hypothesized the occurrence of two subsequent events. The Fi2 deposit suggested the occurrence of Event Eq2 because its base unconformably overlays Fi3 (Fig. 6). Moreover, the evident triangular shape of Fi2 (inset in Fig. 6) and the proximity with fault FA suggest that it represents a colluvial wedge formed after the event Eq2 owing to erosion of the coseismic surface scarp along FA. The thickness of the colluvial wedge is 18 cm, and then the Eq2 event produced a minimum displacement of 36 cm (McCalpin, 2009).

The upslope limit of the colluvial wedge Fi2 coincides with fault FA (Fig. 6). Specifically, the contact between Fi2, in the FA hanging wall and U5, in the FA footwall, appears vertical and sharp. This suggests that the colluvial wedge Fi2 has been cut once again by FA and placed in lateral contact with U5. Otherwise, one would expect that Fi2 has just unconformably overlaid U5, being the product of the fault footwall erosion. Instead, the abrupt lateral contact between Fi2 and U5 was represented by the FA plane. This hence suggests a further episode of activation of the fault, which we name Eq1, that occurred after the deposition of Fi2 and that displaced Fi2 itself.

Due to human plowing activities, a recent extended erosional process ES2 did not permit the maintenance of the first centimeters of the most recent stratigraphic succession (Fig. 7g), preventing the accurate determination of the thickness of the youngest units and then the paleoevent displacement measurements. Nevertheless, if we consider the best-preserved unit U5 outcropping on the northern wall of TA, the minimum thickness of U5 is 50 cm at the footwall and 100 cm at the hanging wall (see Fig. 6). Based on the displaced U5–U6 stratigraphic boundary, we estimated a cumulated minimum offset of ~ 140 cm associated with fault FA (Fig. 7h). This minimum offset should be considered a cumulative of the four events.

3.2.3 Faulting events of trench TB

Trench TB exposes the same stratigraphy of trench TA (Figs. 5 and 6), having at the base a well-stratified slope deposit (unit U1) directly lying under unit U3 (Fig. 8). Unit U1 comprises carbonate stratified fan gravels containing orange, sandy levels 20 cm thick dipping 15°. The more recent stratigraphic sequence fits the observation of the units of trench TA well, except for unit U2, which is not present as it is localized only in the upper part of trench TA, close to the bedrock fault plane. Based on the identified stratigraphic contact, units U4–U5–U6–U7 have thicknesses of 100, 20–60, 90–100, and 20–30 cm, respectively.

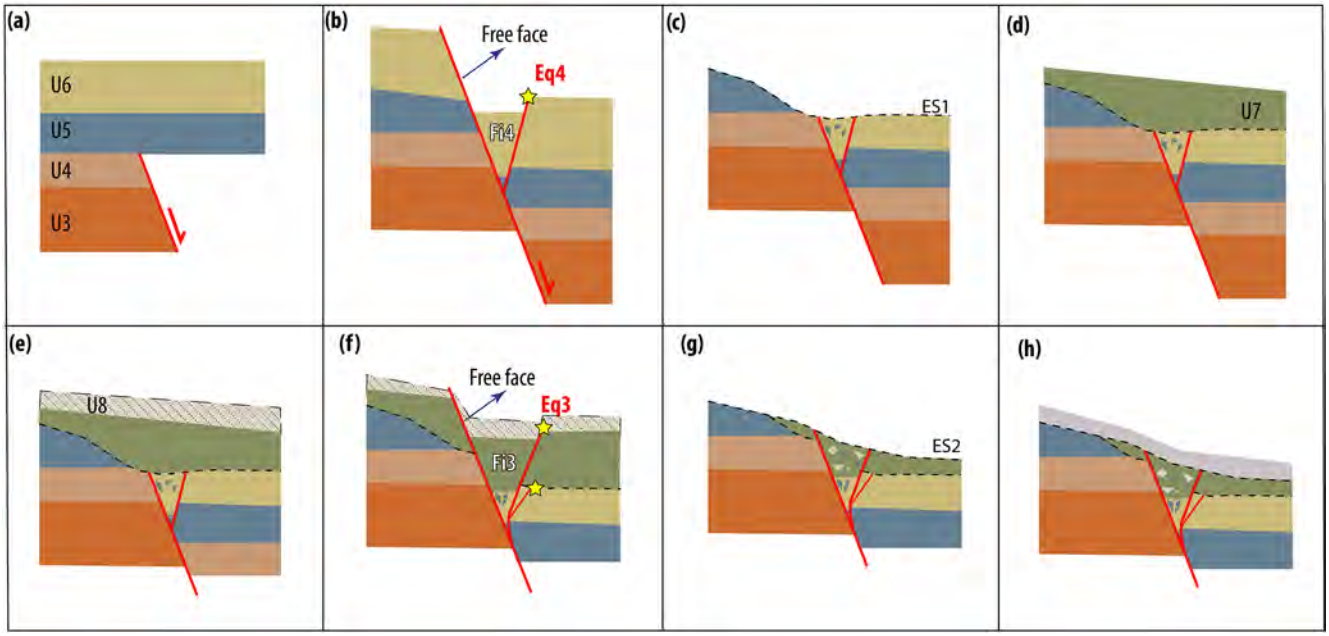

Figure 7. (a–h) Illustrations showing the structural and stratigraphic development of the exposures of the southern wall of trench TA at the FA fault zone (Fig. 6). These illustrations assume that the stratigraphy before U5 was pre-faulted, and the fissure was developed and infilled following the earthquake faulting events, Eq4 and Eq3 (yellow stars).

Trench TB exposed three normal faults arranged synthetic to the principal Mt. Morrone Fault. Fault FB is defined by the contact of units U1–U3 at the footwall with units U4–U5 at the hanging wall, which allows its high-angle geometry recognition. The significant increasing of the thickness of U4 (up to 140 cm) might be related to its involvement in the fault zone between FB and FA. The normal fault FA is instead defined by a nearly vertical, slightly E-dipping, pseudo-reverse fault and is also related to a buried fissure that shows a maximum opening of 65–70 cm, extending for the entire outcrop of the trench (160 cm height).

The arrangement of the material that filled the fissures suggests collapse material coming from hanging walls and/or footwall blocks. Similarly to trench TA, the infilling material is composed of two sediment types, respectively related to different displacement events. As in trench TA, the Fi4 fracture infilling related to the Eq4 event is grey silty sand with the presence of 1 cm clasts diminishing upward, whereas Fi3, related to the Eq3 event, is composed of units U6–U7 as parent material and by a 20 cm thick band of dark-brownish organic material bordering the outer wall of the fissure and filling the central portion. This band suggests the erosion of a paleosol previously overlying the U7 unit located both in the footwall and in the hanging wall block of this fault, i.e., unit U8 mentioned in the discussion of the TA trench. The southern TB trench wall (Fig. 8) shows a well-developed open fissure 60 cm wide, suggesting that Eq3 has been a significant event in terms of surface faulting. Fi3 appeared faulted along FA, as testified by the sharp and almost vertical contact with U4. If Fi3 had not been faulted again along FA, the upslope flank of the large fracture infilled by Fi3 would have been smoothed and upward convex, due to the erosion of the flank of the fracture, with a geometry comparable to its downslope flank (named as "buried fissure wall" in Fig. 8). Lastly, the southern wall of trench TB displays a secondary fault FA1, located 150 cm basinward from FA. It is defined by a 50 cm deep fissure, filled by dark sediments (presumably the same as unit Fi3, i.e., unit U8). The entire sequence is truncated at the top by the anthropogenic erosional surface (ES2) and sealed by the thin-plowed soil.

3.2.4 Evidence of ancient human activities from trench TB

Further evidence collected within trench TB corroborates ancient human activities along this sector of the Mt. Morrone slope, as suggested by the above-mentioned boulder found juxtaposed on the FA scarp (see Fig. 6). At the western end of the northern wall of trench TB, huge rock masses roughly superposed to one another were found during the excavation, the biggest of which was more than 1 m long and about 0.5 m large and thick. A dark-brownish sandy matrix surrounded the boulders (Fig. 9a). The boulders and the matrix filled an ancient excavation cut into unit 6, thus representing a cultural unit (henceforth named CU1; Fig. 9b). We then proceeded with a archaeological-like stratigraphic investigation, that is, by gradually removing each layer to investigate the vertical and horizontal relationship between the cultural unit

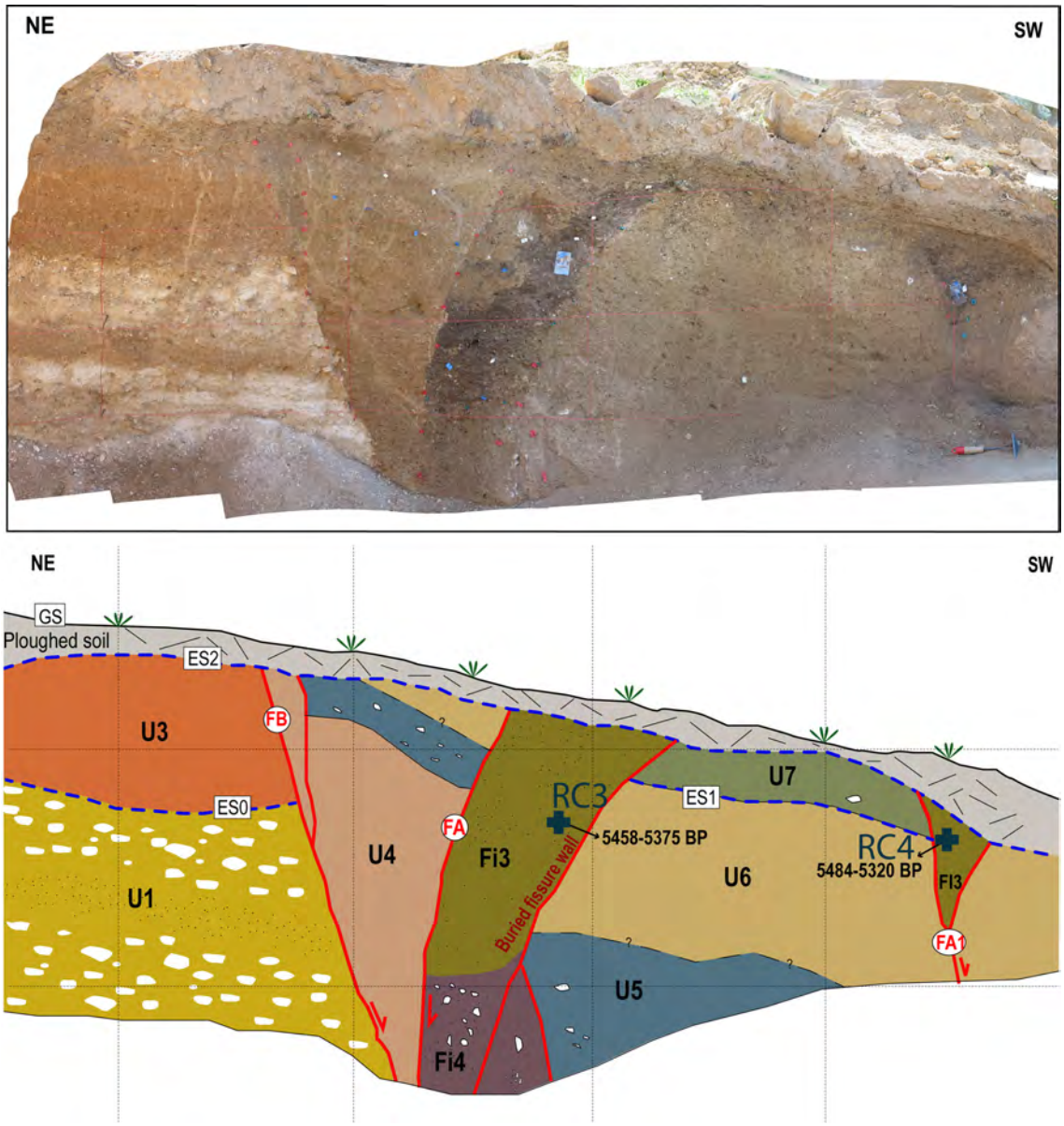

Figure 8. Above: orthophoto mosaic of the southern wall of trench TB, from Agisoft PhotoScan. Below: stratigraphic log of the wall. Unit names and faults are indicated in the figure and referred to in Table 1. ES: erosional surface; GS: ground surface. The samples' position is indicated with a blue cross. Each grid is 100 cm.

and the natural ones. This allowed us to achieve more constraints for the stratigraphy and, hence, for the fault activity (see Gori et al., 2017, about these stratigraphic investigations for paleoseismological analyses). We found evidence that CU1 was overlaid and crosscut by a younger cultural unit (henceforth named CU2; Fig. 9c and d) that was made by a layered deposit of alternating beds, a few centimeters thick, of well-sorted, clast-supported fine carbonate gravel and brownish sandy layers. This unit filled a further ancient excavation made within CU1 (Fig. 9c). Such archaeological-like investigations allowed us to unravel the relationship between the two uncovered cultural units and the fault planes exposed along the trench walls. As shown in Fig. 9b, CU1 is superimposed to the Fi3 infilling of the secondary fracture related to FA1 (Fig. 9d), meaning that CU1 was "settled" after the occurrence of Eq3. In turn, both CU1 and CU2 were affected by another event of activation of FA1, as the continuity of the CU1 boundary is interrupted by the fracture and the materials of CU2 partly fill the void which formed with the displacement along FA1 (Fig. 9d).

In terms of chronology, archaeological investigations done in the past decades revealed human presence along this sector

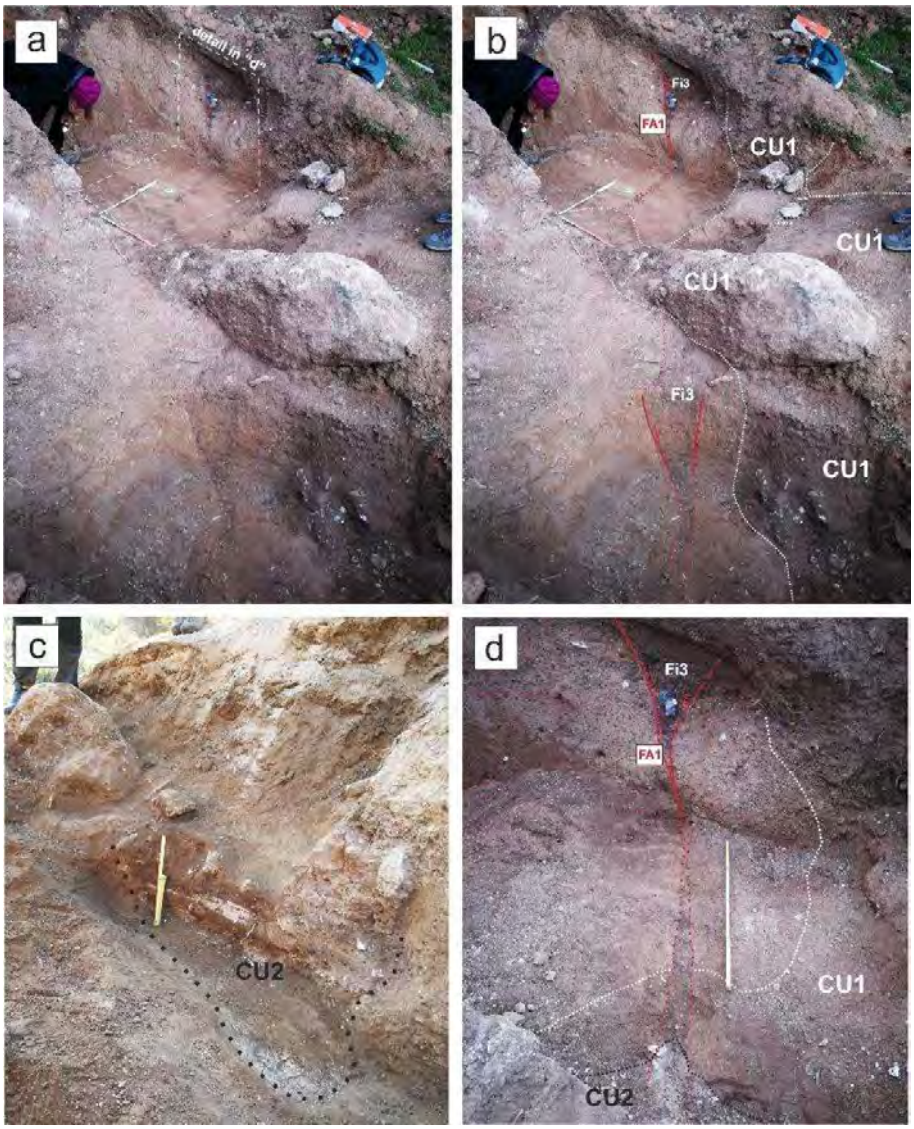

Figure 9. **(a)** SW end of trench TB, where two anthropic units, CU1 and CU2, were found. **(b)** Fault planes FA1 (red lines) that displaced the natural and cultural units; the boundaries of unit CU1 are marked by a dotted white line. **(c)** Close-up view of cultural unit CU2, whose limits are outlined by the dotted black line. **(d)** Close-up view of the southern portion of the SE wall of trench TB that shows the relationship between the fault and the natural and cultural units; CU1 cross-cuts the former fracture formed along FA1, but the fault plane and associated fracture (red lines) displaced the cultural units CU1 and CU2 during an activation event of FA1 subsequent to CU2 deposition. The boundaries of units CU1 and CU2 are marked by dotted white and black lines, respectively.

of the Mt. Morrone SW slope since at least the Bronze Age. In light of this, just upslope of the trenching site, archaeological remnants of an ancient, fortified settlement of local pre-Roman, Italic populations were already well known. These are represented by traces of ancient walls made of polygonal masonry that bounds the top of a relief known as *Colle delle Fate*. This fortified settlement belongs to a series of fortified sites found in this part of the central Apennines and aged in seventh–fourth century BCE, likely around the fourth century BCE, when such fortified structures represented the pivotal centers for the territorial organization and management in the late pre-Roman age (Mattiocco, 1981; Van Wonterghem, 1984). Although we could not distinguish which period the unearthed cultural units belong to, we can stress that they can be attributed to a period not earlier than the Bronze Age; this might also be valid for the boulder daylighted in TA.

3.3 The TC and TD trenches

3.3.1 Stratigraphic setting of TC and TD

The excavations of the two further trenches TC and TD revealed a stratigraphic sequence different from that in trenches TA and TB. It was made by a series of colluvial deposits that we distinguished from one another by the abundance of carbonate clasts, the quantity of clay in the matrix, and the color of the matrix itself. We distinguished three main units (from the oldest to the youngest: unit U1, unit U2, and unit U3). Unit U1 was made by different colluvial bodies that experienced intense deformation induced by fault activity, causing local mixing that hindered a more detailed stratigraphic distinction. Fault activity also placed U3 into contact with U2 and U1 along different fault branches.

Two charcoal shards collected in U2 and U3, of trench TC (southern wall), provided radiocarbon ages of 4460 ± 30 years BP and 3610 ± 30 years BP, respectively (RC6 and RC5 in Table 1), thus testifying to the Late Holocene age of the youngest stratigraphic sequence exposed. The very recent age of the sequence is also confirmed by the presence of a pottery shard in unit U2, whose size and state of preservation hindered archaeological determination (Fig. 10).

In trench TD, the erosional surface ES2, which in trench TC separated U3 from the cultivated soil, cut through the whole stratigraphic sequence, removing U3 almost entirely. Only a tiny portion of U3 remained, so the plowed ground directly overlaid unit U1 along most of the trench (Fig. 11).

3.3.2 Faulting events of TC and TD

Except for the plowed soil, all units were displaced and deformed by the main fault plane and by a set of synthetic and antithetic faults (Figs. 10 and 11). The relationship between the stratigraphic sequence and the fault planes revealed at least two faulting events. The oldest one was responsible for displacing units U1 and U2, placed in contact by fault FH. The event occurred before the deposition of unit U3, which sealed the faulting event. The youngest event displaced unit U3 along the main bedrock fault plane and fault FA and caused a minimum offset of unit U3 of about 1 m in trench TC (Fig. 10). In trench TD, U3 was only displaced by the main fault plane with a minimum offset of 15–20 cm.

4 Discussion and conclusion

Our paleoseismological study was performed south of the Roccacasale village, on the central portion of the Mt. Morrone fault, showing that the basin-bounding fault is a fault with evidence of activity during the Late Pleistocene–Holocene. The paleoseismic study highlighted a 15 m wide zone of deformation associated with two primary fault zones: the bedrock fault plane zone and a fault zone corresponding to a morphological fault scarp, related to synthetic and antithetic fault branches. Paleoseismological trenching across this fault scarp has identified the presence of at least four surface faulting paleoevents involving Late Holocene colluvial deposits.

4.1 Evidence and timing of past earthquakes

The bulk of the observations we made in the trenches allowed us to define the most recent events of activation of the fault. Based on the available age constraints correlated among the four trenches, analyzing the stratigraphic sequences and utilizing the radiocarbon dating as the "terminus post quem" (that is, charcoal fragments or organic matter dated are contained within or are the matrix of detrital colluvial/slope-derived sediments, thus implying that the age obtained is not the age of deposition of the stratigraphic unit, but it predates sedimentation), the occurrence of the four identified faulting events can be defined (Fig. 12).

The oldest earthquake faulting event Eq4 was observed in trench TA, and, according to the interpretation of the event horizon, it predates the emplacement of unit U7. Unit U7 is a colluvial deposit, associated with vertical free-face dismantling; the charcoal embedded in the deposit provides a date of the U7 deposition after 5830–5749 years BP. Therefore, although we do not have chronological constraints of the Eq4 event, we can affirm that the oldest event horizon is sealed by colluvium deposited after 5.8 ± 0.4 kyr BP. As highlighted before, the age of the charcoal in the colluvial unit is not the age of the deposition, but it predates the deposition.

The Eq3 event is observed in both trenches TA and TB (see Figs. 6 and 8), and its chronology was constrained by dating charcoals on trench TB. The ages of the organic material filling the two fissures related to the faults FA and FA1 (trench TB, Fig. 8) are comparable (5458–5375 and 5424–5320 years BP, respectively), and both confirm the contemporaneous occurrence of Eq3 event after this age. The penultimate retrieved event (Eq2) of this fault is observed both on trench TA by the colluvial wedge Fi2 (dated post 4985–4862 years BP) and on trench TC by the faulting evidence of unit U2 (dated post 4430–4490 years BP). Considering the charcoal dating more reliable than the bulk age, the best constraint of event Eq2 has been retrieved by dating the charcoal from unit U2 of trench TC, which provides a post quem age for the penultimate Eq2 event of 4.4 ± 0.3 kyr BP. The fact that FA1 affected the cultural units CA1 and CA2 (not earlier than the initial Bronze Age, i.e., about 3700–3600 BP in the central Apennines; e.g., Silvestri, 2016; Sect. 3.3.2) corroborates the occurrence of a faulting event after Eq3 that re-activated fault FA1.

The most recent event, Eq1, is observed in trench TA (northern wall) by the faulted colluvial wedge (Fi2) and in trench TC where its occurrence is testified by the displacement of unit U1, producing 1 m minimum surface displacement. The chronology of Eq1 can be retrieved by the charcoal found in the deposit of TC, which yielded an age of 3580–

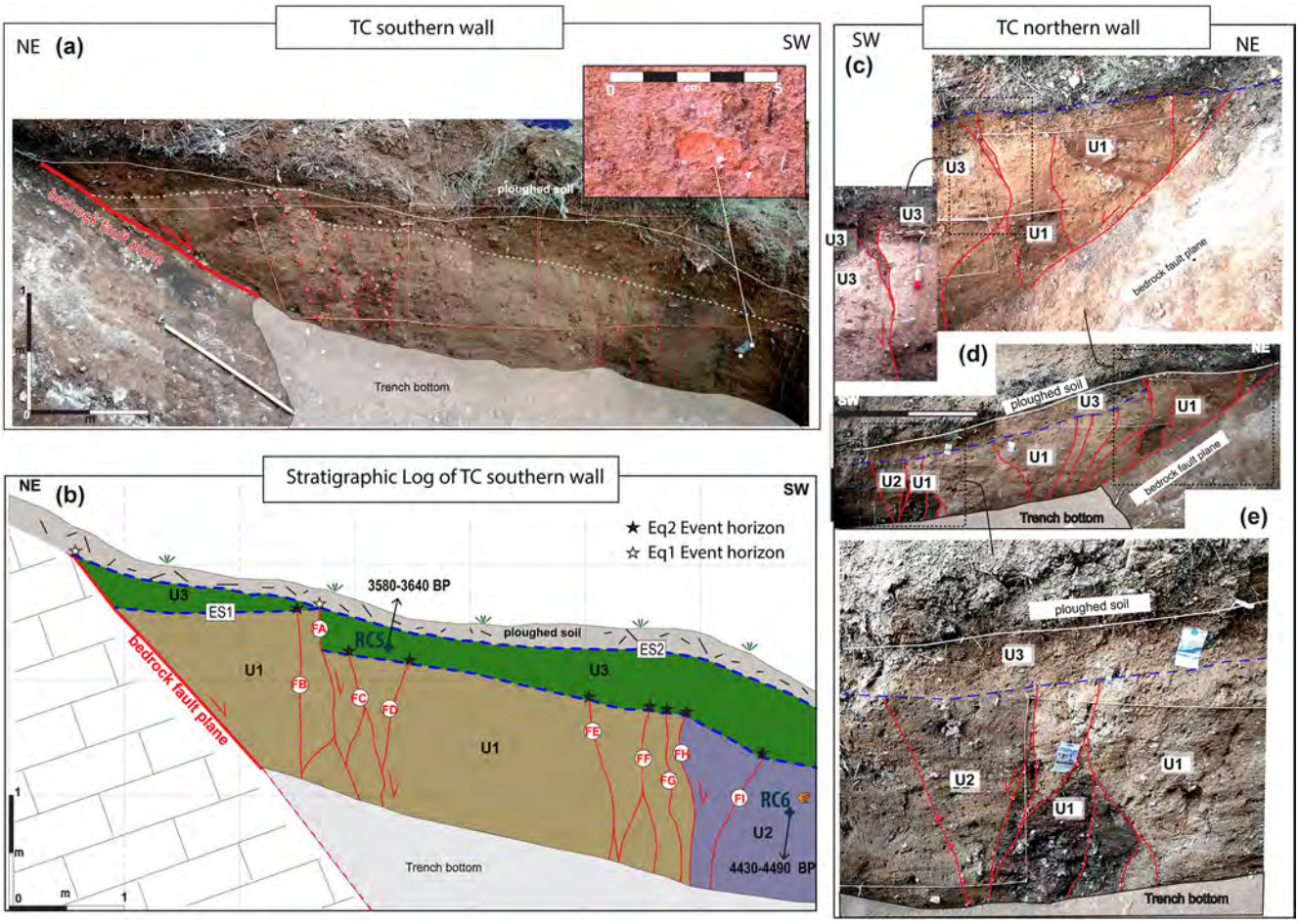

Figure 10. **(a)** Picture of the southern wall of trench TC and **(b)** the related stratigraphic log scheme; red lines mark the fault planes. Stratigraphic units U1, U2, and U3: colluvial units, made of carbonate angular clasts in a sandy and sandy-clayey, brownish, greyish, and yellowish matrix. The pottery shard found within unit U2 is shown in the inset. **(c)** Picture of the northern wall of trench TC. The stratigraphic units are the same as the southern wall; red lines mark the fault planes. Panels **(d)** and **(e)** are close-up views of the fault zones. ES: erosional surface. The picture of the pottery shard found within unit U2 is shown in the inset of **(a)**.

3640 years BP, defining that Eq1 occurred after this age. In summary, based on interpretations and dating from the four investigated trenches, the basin-bounding fault of the MMF has undergone at least three seismic events over the last approximately 5500 years.

4.2 Comparison with previous paleoseismological investigation

The comparison with the previous paleoseismological investigation of Galli et al. (2015), performed at the northern tip of the fault (close to the Popoli village), allows a good time constraint of the events that occurred over the Holocene and provides a well-defined scenario of the rupturing occurrence along the basin-bounding fault. All the paleoseismological investigations, both ours and those of Galli et al. (2015), have been performed on the Sulmona basin-bounding fault, i.e., the western splay of the MMF system. The four trenches near the Popoli village, from Galli et al. (2015), have shown the presence of a fault offsetting Quaternary deposits and recording, overall, four events over the last ∼ 9000 years BP (Fig. 13).

Galli et al. (2015) reported the ultimate event (Eq1g) in ∼ 2000 years BP, corresponding to the second century CE earthquake, also individuated by the former archaeoseismological investigations (Galadini and Galli, 2001; Ceccaroni et al., 2009). In the present study, the ultimate detected event (Eq1) has been recognized in the trenches TA and TC of Roccacasale, which constrained the event after 3610 ± 30 years BP. Such an event produced a minimum recorded vertical displacement of 1 m, suggesting an activation of the entire fault, able to produce widespread damages to villages, like those archaeoseismologically inferred (Ceccaroni et al., 2009).

The penultimate event was observed at the Popoli trenches where Galli et al. (2015) estimated 185 cm of vertical displacement (Eq2g). The occurrence of the paleoearthquake

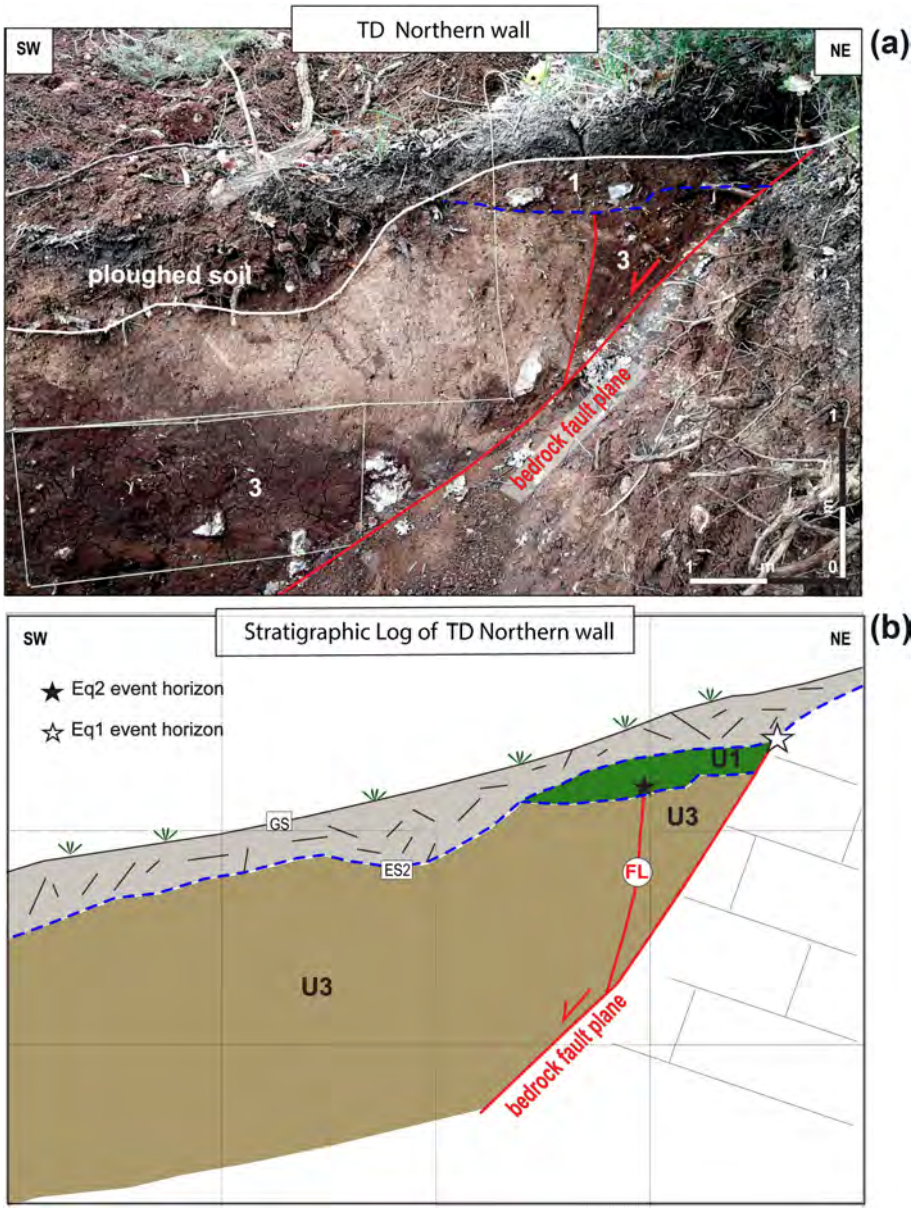

Figure 11. **(a)** Picture of the northern wall of trench TD and **(b)** the related stratigraphic log scheme; red lines mark the fault planes. The stratigraphic units are the same as described in Fig. 9. ES: erosional surface; GS: ground surface.

was found after 5280–4970 years BP, determined by detrital charcoal in colluvial units right below the coseismic fissure. In our trenches, the penultimate event Eq2 has been identified with an age post of 4490–4430 years BP, and so it shows a shorter time window than the Popoli site Eq2g event. The lack of a well-constrained slip per event on the Roccacasale site prevents the comparison in terms of displacements between the two penultimate events (Eq2g and Eq2); hence, two open hypotheses can be made for the comparison between the trench sites. The first hypothesis is to consider Eq2g the same as Eq2 so that the coseismic throw of 36 cm retrieved in the Roccacasale should be considered a minimum offset per event for the investigated splay (and indeed for the whole MMF). The second scenario is that Eq2 is an event not observed in the Popoli trenches due to (i) the lack of record in the investigated trenches or (ii) the lack of coseismic faulting at the northern MMF sector (therefore the low vertical displacement recorded on trench TA may indicate an event with magnitude lower than Eq1). In this case, Eq2g would correspond to the third-last event recognized in the Roccacasale site, Eq3 dated post 5458–5375 years BP. At the Roccacasale site, we retrieved an opening fissure measurement of 70 cm related to the Eq3 event, which is comparable to the opening values observed in the Popoli site (100 cm).

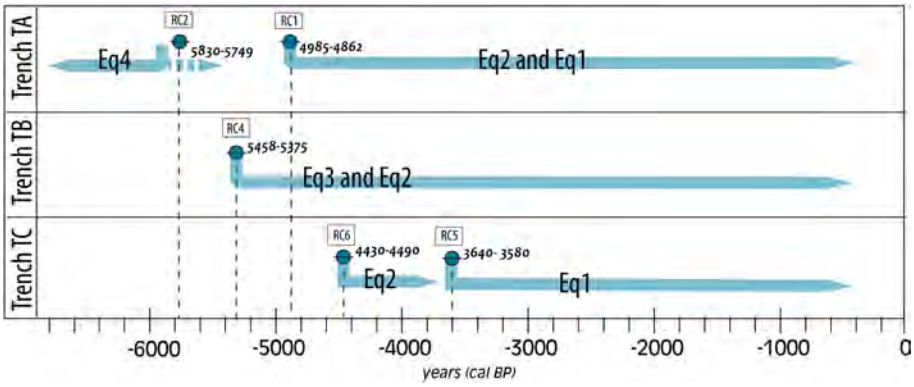

Figure 12. Chronogram of the surface-rupture events identified from within the TA–TB–TC trenches. Each radiocarbon sample is indicated by the blue circle, labeled, and reported with its 2σ calibrated interval. Horizontal blue arrows point to the assumed paleoevent age of occurrence as deduced from the post quem samples age (see text for further details).

Considering the similar topographic conditions of the two sites, such similar opening values might suggest the occurrence of the same triggering event in terms of magnitude indeed. Thus, the Eq3 event should reasonably correspond to Eq2g, and then it can be an event that occurred after 5280–4970 years BP.

Moreover, speleoseismological studies around 10 km conducted to the east of the MMF by Di Domenica and Pizzi (2017) in the Cavallone cave (close to the Majella Massif; see Fig. 1) revealed the occurrence of a seismic-induced gravitational collapse of stalagmites in the cave, whose age was constrained between 4815–4755 and 4675–4645 years BP. Again, the authors dated a well-preserved buried wood (the portion of a Quercus ilex trunk) incorporated within a seismic-induced landslide body, close to the Palena village, corresponding to an age of 5445–5300 years BP. Although the authors did not assess the simultaneous occurrence of these two events for certain (the gravitational collapse of the stalagmites and the landslide occurrence), the comparable age range of these exceptional and catastrophic events suggests that both the cave damage and the rock avalanche may represent the effects of strong paleoearthquakes. The collapse of the speleothem suggests the occurrence of a strong earthquake between 4.8–4.6 kyr BP in the region but not necessarily associated with the MMF activation. On the other hand, the chronological constraints related to the Palena rock avalanche indicate an event that occurred after 5.4–5.3 kyr BP, which results in good agreement with the chronologies of the Eq3 event retrieved by our paleoseismological study. Furthermore, both the newly presented and the Galli et al. (2015) paleoseismological evidence of the ruptures might also indicate the occurrence of a local event stronger than 6.5 (e.g., Galli et al., 2015), caused by a larger seismogenic source of the region. In light of this, it must be underlined that this part of the Maiella massif in which the speleothems' collapse was found was affected by the 1706 earthquake ($M \sim 6.8$), whose seismogenic source is still undefined and tentatively associated with a reverse structure (De Nardis et al., 2008; Galli and Pallone, 2019).

By dating the organic materials found directly below a colluvial wedge on the Popoli trenches, it was determined that a third event, Eq3g, occurred after 8540–8370 years BP. Eq4 observed in our study can be compared to this event. Based on our analysis of a charcoal sample from the colluvium (U7) that was deposited after Eq4 at 5830–5749 years BP, we should assume that Eq4 was an event that occurred before this age. Thus, it can agree with Eq3g. In the Popoli trenches, a final event called Eq4g was observed and dated to after 9090–8980 years BP.

Overall, the new available chronological constraints of the four paleoearthquakes revealed by the Roccacasale trenches along with the integration of the existing paleoseismological and archaeoseismological data (i.e., Galadini and Galli, 2001; Ceccaroni et al., 2009; Galli et al., 2015; Di Domenica and Pizzi, 2017) allow a better definition of the Holocene behavior the MMF. By matching the observations and combining the evidence from the literature, the last fault activation we identified is consistent with the most recent event in the second century CE (Eq1) defined by previous studies, the penultimate event occurred after 4.4 kyr BP (Eq2), the third-last event took place after 5.4–5.3 kyr (Eq3; between 4.8 and 4.6 kyr BP if coincident with the cave's collapse), and the last event occurred presumably before 5.8–5.7 kyr BP and after 8.5–8.4 kyr BP.

Considering the evaluated constraints for the faulting events, we defined an average recurrence time for characteristic earthquakes by considering the last three events that occurred over the last 5.4 kyr (for which we identified a post quem age). By dividing this interval by the three events (i.e., Eq3, Eq2, and Eq1) we determined an average recurrence interval of 1800 years for M 6.5–7-like events (based on the regressions of Wells and Coppersmith, 1994). This result agrees with the average recurrence time in the central Apennines (Galadini and Galli, 2000). On the other hand,

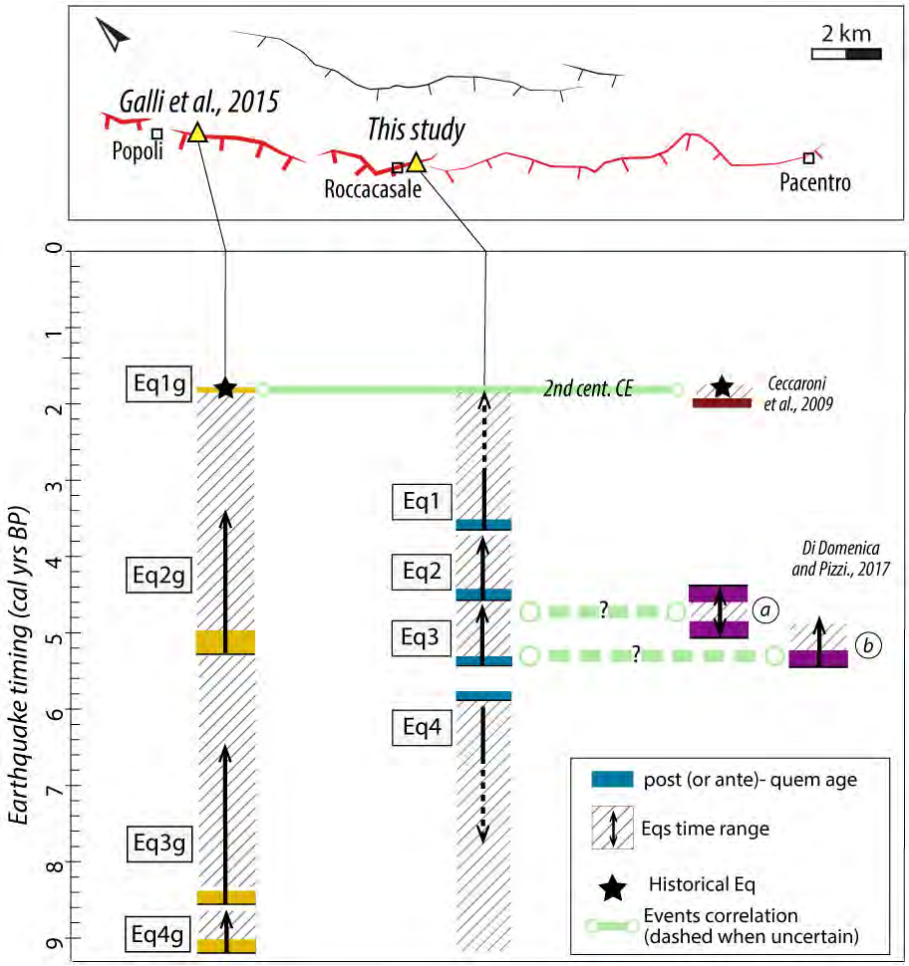

Figure 13. Chronogram of the surface-rupture events for the MMF. In the lower panel, events from dating in literature are reported: yellow from Galli et al. (2015), purple from Di Domenica and Pizzi (2017), and red from Ceccaroni et al. (2009). The two age intervals from Di Domenica and Pizzi (2017) are from **(a)** speleothem radiocarbon dating (i.e., ante and post quem termini) and **(b)** radiocarbon dating of wood embedded in a rock avalanche (see the main text for further details). Data from this study are indicated in blue. Each colored rectangle is a radiocarbon sample, and the height reports its 2σ calibrated interval of age. Black arrows indicate the range of the event occurrence constrained by the post quem data. The striped rectangles indicate the range of time-occurrence uncertainty related to each event. Green lines indicate the events correlations (dashed when hypothesized because not directly correlated to on-fault data).

preceding studies show the occurrence of four events over the last 9 kyr and suggest an average recurrence interval of 2400 years (Galli et al., 2015). Therefore, considering that the elapsed time since the last event Eq1 is $\sim$1850 years (which recorded at both sites a minimum displacement of 1 m), the newly determined average recurrence interval has important implications as it reveals that the fault might be closer to failure. Therefore, the new data should be carefully considered and included in the estimations of the probability of earthquake occurrence in central Italy.

In conclusion, this study corroborates the findings available in the literature, while refining and extending the chronological record of the paleoseismic history of the MMF, particularly for the past 5000–6000 years. This is a crucial aspect for assessing earthquake probability in the central Apennines. In this context, the MMF is considered a "silent" active and seismogenic fault (Galadini and Galli, 2000), meaning that it represents a major tectonic structure of which the elapsed time since the last activation approximates the fault's average recurrence interval. Specifically, our results have shortened the previously defined mean recurrence interval of the MMF to approximately 1800 years, which corresponds to the time elapsed since its last activation. In this context, the 2016 seismic sequence in central Italy is worth mentioning. Prior to 2016, the Mt. Vettore–Bove fault was deemed a major active seismogenic fault in the central Apennines, potentially responsible for M 6.5–6.6 earthquakes (based on geological and paleoseismological studies; Galadini and Galli, 2003), and it was also considered "silent" by the cited authors, similar to other active faults in

the central Apennines, including the MMF. The 2016 seismic sequence confirmed this hypothesis, as it was caused by the activation of the Mt. Vettore-Bove fault, which fully ruptured, generating three major seismic events, the strongest of which occurred on 30 October 2016, with a magnitude of M_w 6.5 (e.g., Chiaraluce et al., 2017; Cheloni et al., 2019; Civico et al., 2018).

The 2016 central Italy seismic sequence thus demonstrated the reliability, efficacy, and necessity of this kind of study on active faults, which are primarily based on thorough geological investigations aimed at defining fault activity over long time spans (from tens to hundreds of thousands of years) and detailed paleoseismological analyses aimed at understanding fault behavior over the past few thousand years. This is particularly significant in areas like the central Apennines, where numerous towns, inhabited by thousands of people, are located, encompassing cultural heritage and productive activities. Regarding the MMF, its potential to produce strong seismic events (with magnitudes of up to 6.5–7; Bordoni et al., 2023), coupled with the absence of recent historical earthquakes and the newly defined average recurrence interval, confirms it as one of the most problematic active tectonic structures in this part of Italy.

Data availability. This work does not include any external dataset sources; all the data are included in the main text (i.e., Sect. 3 and Table 1) or in the Supplement.

Supplement. The supplement related to this article is available online at https://doi.org/10.5194/se-16-275-2025-supplement.

Author contributions. Conceptualization, AP; data acquisition and field analysis, IP, AP, SG, EF, MM, MS, and FG; data curation, IP, SG, and EF; figure production, IP and SG; GIS mapping and writing (original draft preparation), IP, SG, and EF; supervision and project administration, AP and FG; funding acquisition, AP and FG.

Competing interests. The contact author has declared that none of the authors has any competing interests.

Disclaimer. Publisher's note: Copernicus Publications remains neutral with regard to jurisdictional claims made in the text, published maps, institutional affiliations, or any other geographical representation in this paper. While Copernicus Publications makes every effort to include appropriate place names, the final responsibility lies with the authors.

Acknowledgements. This work has been funded by the Italian Ministry for Education, University and Research (MIUR) (ex60% grants to Alberto Pizzi). The 2018 mayor of Roccacasale, Enrico Pace, is acknowledged for his interest in scientific study. Special thanks are given to geologists Mimmo Trotta, Catia Di Nisio, and Tania Campea, who are recognized for their support and help in the field and logistics. We also acknowledge the two reviewers Francesco Iezzi and Nasim Mozafari Amiri for helping to improve the manuscript.

Financial support. This research has been supported by the Italian Ministry of Education, University and research (MIUR) (grant no. ex 60% grants).

Review statement. This paper was edited by Kei Ogata and reviewed by Francesco Iezzi and Nasim Mozafari Amiri.

References

Benvenuti, M. and Martini, I. P.: Analysis of Terrestrial Hyperconcentrated Flows and their Deposit, in: Flood and Megaflood Processes and Deposits, edited by: Martini, I. P., Baker, V. R., and Garzón, G., 167–193, https://doi.org/10.1002/9781444304299.ch10, 2009.

Boccaletti, M., Ciaranfi, N., Cosentino, D., Deiana, G., Gelati, R., Lentini, F., Massari, F., Moratti, G., Pescatore, T., Ricci Lucchi, F., and Tortorici, L.: Palinspastic restoration and paleogeographic reconstruction of the peri-Tyrrhenian area during the Neogene, Palaeogeogr. Palaeocl., 77, 41–42, https://doi.org/10.1016/0031-0182(90)90097-Q, 1990.

Bordoni, P., Gori, S., Akinci, A., Visini, F., Sgobba, S., Pacor, F., Cara, F., Pampanin, S., Milana, G., and Doglioni, C.: A site-specific earthquake ground response analysis using a fault-based approach and nonlinear modeling: The Case Pente site (Sulmona, Italy), Eng. Geol., 314, 106970, https://doi.org/10.1016/j.enggeo.2022.106970, 2023.

Bosi, C. and Bertini, T.: Geologia della media valle dell'Aterno, Mem. Soc. Geol. Ital., 9, 719–777, https://www.socgeol.info/it/fascicoli/?t=Memorie&y=1970&v=9 (last access: April 2025), 1970.

Calamita, F. and Pizzi, A.: Tettonica quaternaria nella dorsale appenninica umbro-marchigiana e bacini intrappenninici associati, http://193.204.8.201:8080/jspui/handle/1336/541 (last access: April 2025), 1992.

Bosi, C., Galadini, F., Giaccio, B., Messina, P., and Sposato, A.: Plio-Quaternary continental deposits in the Latium-Abruzzi: the correlation of geological events across different intermontane basins, Il Quaternario, 16, 55–76, 2003.

Cavinato, G. P. and Miccadei, E.: Pleistocene carbonate lacustrine deposits: Sulmona basin (central Apennines, Italy), Lake Basins through Space and Time, Am. Assoc. Pet. Geol. Stud. Geol., 46, 517–526, 2000.

Cavinato, G. P., Cosentino, D., De Rita, D., Funiciello, R., and Parotto M.: Tectonic-sedimentary evolution of intrapenninic basins and correlation with the volcano-tectonic activity in central Italy, Mem. Descr. Carta Geol. d'It., 49, 63–76, 1994.

Ceccaroni, E., Ameri, G., Gómez Capera, A. A., and Galadini, F.: The 2nd century AD earthquake in central Italy: Archaeoseismo-

logical data and seismotectonic implications, Nat. Hazards, 50, 335–359, https://doi.org/10.1007/s11069-009-9343-x, 2009.

Cheloni, D., Falcucci, E., and Gori, S.: Half-graben rupture geometry of the 30 October 2016 M_W6.6 Mt. Vettore-Mt. Bove earthquake, central Italy, J. Geophys. Res.-Sol. Ea., 124, 4091–4118, https://doi.org/10.1029/2018JB015851, 2019.

Chiaraluce, L., Di Stefano, R., Tinti, E., Scognamiglio, L., Michele, M., Casarotti, E., Cattaneo, M., De Gori, P., Chiarabba, C., Monachesi, G., Lombardi, A., Valoroso, L., Latorre, D., and Marzorati, S.: The 2016 central Italy seismic sequence: a first look at the mainshocks, aftershocks and source models, Seismol. Res. Lett., 88, 757–771, https://doi.org/10.1785/0220160221, 2017.

Ciccacci, S., D'Alessandro, L., Dramis, F., and Miccadei, E.: Geomorphologic evolution and neotectonics of the Sulmona intramontane basin (Abruzzi Apennine, Central Italy), Z. Geomorphol., 118, 27–40, http://geoprodig.cnrs.fr/items/show/89849 (last access: April 2025), 1999.

Cipollari, P. and Cosentino, D.: Miocene unconformities in the Central Apennines: geodynamic significance and sedimentary basin evolution, Tectonophysics, 252, 375–389, https://doi.org/10.1016/0040-1951(95)00088-7, 1995.

Cipollari, P. and Pipponzi, G.: Le "Calciruditi di Calaturo" (Montagna del Morrone): un deposito tardo-orogenico della fine del Pliocene inferiore, Studi Geologici Camerti, Numero Speciale, 1/2003, 73–83, http://193.204.8.201:8080/jspui/handle/1336/859 (last access: April 2025), 2003.

Cipollari, P., Cosentino, D., and Gliozzi, E.: Extension- and compression-related basins in central Italy during the Messinian Lago-Mare event, Tectonophysics, 315, 163–185, https://doi.org/10.1016/S0040-1951(99)00287-5, 1999.

Civico, R., Pucci, S., Villani, F., Pizzimenti, L., De Martini, P. M., Nappi, R., and the Open EMERGEO Working Group: Surface ruptures following the 30 October 2016 M_W 6.5 Norcia earthquake, central Italy, J. Maps, 14, 151–160, https://doi.org/10.1080/17445647.2018.1441756, 2018.

Demangeot, J.: Geomorphologie des Abruzzes adriatiques in Memorie set Documents, Editions du Centre National de la Recherche Scientifique, Paris, 388, 1965.

De Nardis, R., Pace, B., Lavecchia, G., Visini, F., and Boncio, P.: Geological and macroseismic data for seismotectonic purpose: the 1706 Maiella (Abruzzo, Italy) earthquake case study, in: AGU Fall Meeting Abstracts, Vol. 2008, T21B–1946, https://ui.adsabs.harvard.edu/abs/2008AGUFM.T21B1946D/abstract (last access: April 2025), 2008.

Di Domenica, A. and Pizzi, A.: Defining a mid-Holocene earthquake through speleoseismological and independent data: implications for the outer Central Apennines (Italy) seismotectonic framework, Solid Earth, 8, 161–176, https://doi.org/10.5194/se-8-161-2017, 2017.

Doglioni, C.: A proposal for the Kinematic modelling of Wdipping subductions – possible applications to the Tyrrehenian Appennines system, Terra Nova, 3 (issue 4), 423–434, https://doi.org/10.1111/j.1365-3121.1991.tb00172.x, 1991.

DuRoss, C. B., Personius, S. F., Crone, A. J., Olig, S. S., and Lund, W. R.: Integration of paleoseismic data from multiple sites to develop an objective earthquake chronology: Application to the Weber segment of the Wasatch fault zone, Utah, B. Seismol. Soc. Am., 101, 2765–2781, https://doi.org/10.1785/0120110102, 2011.

DuRoss, C. B., Olig, S. S., Lund, W. R., and Schwartz, D. P.: Fault segmentation: New concepts from the Wasatch Fault Zone, Utah, USA, J. Geophys. Res.-Sol. Ea., 121, 1131–1157, https://doi.org/10.1002/2015JB012519 2016.

Ekström, G., Morelli, A., Boschi, E., and Dziewonski, A. M.: Moment tensor analysis of the central Italy earthquake sequence of September–October 1997, Geophys. Res. Lett., 25, 1971–1974, 1998.

Falcucci, E., Gori, S., Bignami, C., Pietrantonio, G., Melini, D., Moro, M., Saroli, M., and Galadini, F.: The Campotosto seismic gap in between the 2009 and 2016–2017 seismic sequences of Central Italy and the role of inherited lithospheric faults in regional seismotectonic settings, Tectonics, 37, 2425–2445, https://doi.org/10.1029/2017TC004844, 2018.

Galadini, F. and Galli, P.: Active Tectonics in the Central Apennines (Italy) – Input Data for Seismic Hazard Assessment, Nat. Hazards, 22, 225–270, https://doi.org/10.1023/A:1008149531980, 2000.

Galadini, F. and Galli, P.: Archaeoseismology in Italy: case studies and implications on long-term seismicity, J. Earthq. Eng., 5, 35–68, 2001.

Galadini, F. and Galli, P.: Paleoseismology of silent faults in the Central Apennines (Italy): The Mt. Vettore and Laga Mts. faults, Ann. Geophys., 46, 815–836, https://doi.org/10.4401/ag-3457, 2003.

Galadini, F. and Messina, P.: Early-Middle Pleistocene eastward migration of the Abruzzi Apennine (central Italy) extensional domain, J. Geodyn., 37, 57–81, https://doi.org/10.1016/j.jog.2003.10.002, 2004.

Galli, P. and Pallone, F.: Reviewing the intensity distribution of the 1933 earthquake (Maiella, Central Italy). Clues on the seismogenic fault, Alpine and Mediterranean Quaternary, 32, 93–100, 2019.

Galli, P., Galadini, F., and Pantosti, D.: Twenty years of paleoseismology in Italy, Earth-Sci. Rev., 88, 89–117, https://doi.org/10.1016/j.earscirev.2008.01.001, 2008.

Galli, P., Giaccio, B., Peronace, E., and Messina, P.: Holocene paleoearthquakes and early-late pleistocene slip rate on the sulmona fault (Central Apeninnes, Italy), B. Seismol. Soc. Am., 105, 1–13, https://doi.org/10.1785/0120140029, 2015.

Ghisetti, F. and Vezzani, L.: Interfering paths of deformation and development of arcs in the fold-and-thrust belt of the central Apennines (Italy), Tectonics, 16, 523–536, https://doi.org/10.1029/97TC00117, 1997.

Giaccio, B., Messina, P., Sposato, A., Voltaggio, M., Zanchetta, G., Galadini, F., Gori, S., and Santacroce, R.: Tephra layers from Holocene lake sediments of the Sulmona Basin, central Italy: implications for volcanic activity in Peninsular Italy and tephrostratigraphy in the central Mediterranean area, Quaternary Sci. Rev., 28, 2710–2733, https://doi.org/10.1016/j.quascirev.2009.06.009, 2009.

Gori, S.: Definition of seismogenic sources in poorly known tectonically active regions of the Italian Peninsula", PhD Thesis, Università degli Studi Roma Tre. Tutor Prof. Francesco Dramis, https://arcadia.sba.uniroma3.it/handle/2307/561 (last access: April 2025), 2010.

Gori, S., Dramis, F., Galadini, F., and Messina, P.: The use of geomorphological markers in the footwall of active faults for kine-

matic evaluation: examples from the central Apennines, Boll. Soc. Geol. Ital., 126, 365–374, 2007.

Gori, S., Giaccio, B., Galadini, F., Falcucci, E., Messina, P., Sposato, A., and Dramis, F.: Active normal faulting along the Mt. Morrone south-western slopes (central Apennines, Italy), International Journal of Earth Sciences, 100, 157–171, 2011.

Gori, S., Falcucci, E., Dramis, F., Galadini, F., Galli, P., Giaccio, B., Messina, P., Pizzi, A., Sposato, A., and Cosentino, D.: Deep-seated gravitational slope deformation, large-scale rock failure, and active normal faulting along Mt. Morrone (Sulmona basin, Central Italy): Geomorphological and paleoseismological analyses, Geomorphology, 208, 88–101, https://doi.org/10.1016/j.geomorph.2013.11.017, 2014.

Gori, S., Falcucci, E., Ladina, C., Marzorati, S., and Galadini, F.: Active faulting, 3-D geological architecture and Plio-Quaternary structural evolution of extensional basins in the central Apennine chain, Italy, Solid Earth, 8, 319–337, https://doi.org/10.5194/se-8-319-2017, 2017.

Iezzi, F., Mildon, Z., Walker, J. F., Roberts, G., Goodall, H., Wilkinson, M., and Robertson, J.: Coseismic Throw Variation Across Along-Strike Bends on Active Normal Faults: Implications for Displacement Versus Length Scaling of Earthquake Ruptures, J. Geophys. Res.-Sol. Ea., 123, 9817–9841, https://doi.org/10.1029/2018JB016732, 2018.

Iezzi, F., Francescone, M., Pizzi, A., Blumetti, A., Boncio, P., Di Manna, P., Pace, B., Piacentini, T., Papasodaro, F., Morelli, F., Caciagli, M., Chiappini, M., D'Ajello Caracciolo, F., Materni, V., Nicolosi, I., Sapia, V., and Urbini, S.: Slip localization on multiple fault splays accommodating distributed deformation across normal fault complexities, Tectonophysics, 868, 230075, https://doi.org/10.1016/j.tecto.2023.230075, 2023.

Lavecchia, G., Brozzetti, F., Barchi, M., Menichetti, M., and Keller, J. V. A.: Seismotectonic zoning in east-central Italy deduced from an analysis of the Neogene to present deformations and related stress fields, Geol. Soc. Am. Bull., 106, 1107–1120, https://doi.org/10.1130/0016-7606(1994)106<1107:SZIECI>2.3.CO;2, 1994.

Manighetti, I., Campillo, M., Bouley, S., and Cotton, F.: Earthquake scaling, fault segmentation, and structural maturity, Earth Planet. Sc. Lett., 253, 429–438, 2007.

Mattiocco, E.: Sulmona: oppidum, civitas, città in Vicende urbanistiche di citta meridionali. Storia Urbana Milano, 27–49, http://openbibart.fr/vibad/index.php?action=getRecordDetail&idt=oba_0601273 (last access: April 2025) 1981.

McCalpin, J. P.; Paleoseismology in extensional tectonic environments, International Geophysics, 95, 171–269, 2009.

Miccadei, E., Barberi, R., and Cavinato, G. P.: La geologia quaternaria della Conca di Sulmona (Abruzzo, Italia centrale), Geologica Romana, 34, 59–86, 1998.

Miccadei, E., Paron, P., and Piacentini, T.: The SW escarpment of Montagna del Morrone (Abruzzi, Central Italy): Geomorphology of a fault-generated mountain front, Geogr. Fis. Din. Quat., 27, 55–87, 2004.

Patacca, E., Sartori, R., and Scandone, P.: Tyrrhenian basin and Apenninic arcs : Kinematic relations since Late Tortonian times, Memorie Della Societa Geologica Italiana, 45, 425–451, 1990.

Peacock, D. C. P. and Sanderson, D. J.: Displacements, segment linkage and relay ramps in normal fault zones, J. Struct. Geol., 13, 721–733, https://doi.org/10.1016/0191-8141(91)90033-F, 1991.

Piccardi, L., Gaudemer, Y., Tapponnier, P., and Boccaletti, M.:. Active oblique extension in the central Apennines (Italy): Evidence from the Fucino region, Geophys. J. Int., 139, 499–530, https://doi.org/10.1046/j.1365-246X.1999.00955.x, 1999.

Pizzi, A. and Pugliese, G.: InSAR-DEM analyses integrated with geologic field methods for the study of long-term seismogenic fault behavior: Applications in the axial zone of the central Apennines (Italy), J. Seismol., 8, 313–329, https://doi.org/10.1023/B:JOSE.0000038454.18706.25, 2004.

Pizzi, A., Falcucci, E., Gori, S, Galadini, F., Messina, P., Di Vincenzo, M., and Sposato, A.: Active faulting in the Maiella massif (central Apennines, Italy), GeoActa, 3, 57–73, 2010.

Pondrelli, S., Salimbeni, S., Morelli, A., Ekström, G., Olivieri, M., and Boschi, E.: Seismic moment tensors of the April 2009, L'Aquila (Central Italy), earthquake sequence, Geophys. J. Int., 180, 238–242, 2010.

Pucci, S., Villani, F., Civico, R., Pantosti, D., Del Carlo, P., Smedile, A., De Martini, P. M., Pons-Branchu, E., and Gueli, A.: Quaternary geology of the Middle Aterno Valley, 2009 L'Aquila earthquake area (Abruzzi Apennines, Italy), J. Maps, 11, 689–697, https://doi.org/10.1080/17445647.2014.927128, 2015.

Pucci, S., Villani, F., Civico, R., Di Naccio, D., Porreca, M., Benedetti, L., Gueli, A., Stella, G., Baccheschi, P., and Pantosti, D.: Complexity of the 2009 L'Aquila earthquake causative fault system (Abruzzi Apennines, Italy) and effects on the Middle Aterno Quaternary basin arrangement, Quaternary Sci. Rev., 213, 30–66, https://doi.org/10.1016/j.quascirev.2019.04.014, 2019.

Puliti, I., Pizzi, A., Benedetti, L., Di Domenica, A., and Fleury, J.: Comparing Slip Distribution of an Active Fault System at Various Timescales: Insights for the Evolution of the Mt. Vettore-Mt. Bove Fault System in Central Apennines, Tectonics, 39, e2020TC006200, https://doi.org/10.1029/2020TC006200, 2020.

Puliti, I., Pucci, S., Villani, F., Porreca, M., Benedetti, L., Robustelli, G., Gueli, A., and Stella, G.: Estimating the long-term slip rate of active normal faults: The case of the Paganica Fault (Central Apennines, Italy), Geomorphology, 415, 108411, https://doi.org/10.1016/j.geomorph.2022.108411, 2022.

Puliti, I., Benedetti, L., Pizzi, A., Fleury, J., Francescone, M., Guillou, V., and Team, A.: Evidence for a constant slip rate over the last ∼40 ka along the Mt. Morrone Fault System in Central Apennines, Tectonics, 43, e2023TC007871, https://doi.org/10.1029/2023TC007871, 2024.

Ramsey, C. B.: Bayesian analysis of radiocarbon dates, Radiocarbon, 51, 337–360, https://doi.org/10.1017/S0033822200033865, 2009.

Reimer, P. J., Bard, E., Bayliss, A., Beck, J. W., Blackwell, P. G., Ramsey, C. B., Brown, D. M., Buck, C. E., Edwards, R. L., Friedrich, M., Grootes, P. M., Guilderson, T. P., Haflidason, H., Hajdas, I., Hatté, C., Heaton, T. J., Hogg, A. G., Hughen, K. A., Kaiser, K. F., and van der Plicht, J.: Selection and Treatment of Data for Radiocarbon Calibration: An Update to the International Calibration (IntCal) Criteria, Radiocarbon, 55, 1923–1945, https://doi.org/10.2458/azu_js_rc.55.16955, 2013.

Rovida, A., Antonucci, A., and Locati, M.: The European Preinstrumental Earthquake Catalogue EPICA, the 1000–1899 catalogue for the European Seismic Hazard Model 2020, Earth Syst.

Sci. Data, 14, 5213–5231, https://doi.org/10.5194/essd-14-5213-2022, 2022.

Servizio Geologico d'Italia: Carta Geologica d'Italia alla scala 1 : 50, 000, F. 369 Sulmona, ISPRA, Roma, https://www.isprambiente.gov.it/Media/carg/369_SULMONA/Foglio.html (last access: April 2025), 2006.

Silvestri, A.: Il villaggio dell'età del Bronzo di Trasacco (AQ), nuovi dati. In: "Il Fucino e le aree limitrofe nell'antichità. Archeologia e rinascita culturale dopo il sisma del 1915", in: Proceedings of the 4th Archaeological Workshop, Avezzano (Italy), 22–23 May 2015, Archeoclub d'Italia, DVG Studio, Avezzano, Italy, 171–184, 2016.

Van Wonterghem, F.: Superaequum, Corfinium, Sulmo. Forma Italiae, Unione Accademica Nazionale, Istituto di Topografia Antica dell'Università di Roma, edited by: Olschki, L., https://www.olschki.it/libro/9788822232618 (last access: April 2025), 1984.

Vignaroli, G., Rossetti, F., Petracchini, L., Argante, V., Bernasconi, S. M., Brilli, M., Giustini F., Tsai-Luen, Y., Chuan-Chou S., and Soligo, M.: Middle Pleistocene fluid infiltration with 10–15 ka recurrence within the seismic cycle of the active Monte Morrone Fault System (central Apennines, Italy), Tectonophysics, 827, 229269, https://doi.org/10.1016/j.tecto.2022.229269, 2022.

Vittori, G. P. and Cavinato, E. M.: Active Faulting Along the Northerneastern edge of the Sulmona Basin, Central Appennines, Italy, in: Perspectives in Paleoseismology, 115–125, ISBN 0-89716-563-2, 1995.

Walsh, J. J. and Watterson, J.: Distributions of cumulative displacement and seismic slip on a single normal fault surface, J. Struct. Geol., 9, 1039–1046, https://doi.org/10.1016/0191-8141(87)90012-5, 1987.

Wells, D. L. and Coppersmith, K. J.: New empirical relationships among magnitude, rupture length, rupture width, rupture area, and surface displacement, B. Seismol. Soc. Am., 84, 974–1002, 1994.

Zavala, C.: Hyperpycnal (over density) flows and deposits, Journal of Palaeogeography, 9, 17, https://doi.org/10.1186/s42501-020-00065-x, 2020.